Title
Mechanisms of peroxide sensing using phthalocyanine organic thin film transistor arrays

Author
Kappe, Erik Dennis

Publication Date
2011

Peer reviewed|Thesis/dissertation

UNITVERSITY OF CALIFORNIA, SAN DIEGO

Mechanisms of Peroxide Sensing using Phthalocyanine Organic Thin Film Transistor Arrays

A Thesis submitted in partial satisfaction of the requirements for the

degree Master of Science

in

Chemistry

by

Erik Dennis Kappe

Committee in charge:

Professor Andrew Kummel, Chair

Professor Douglas Magde

Professor William Trogler

2011

The Thesis of Erik Dennis Kappe is approved and it is acceptable in quality and form for publication on microfilm and electronically:

Chair

University of California, San Diego

2011

DEDICATION

This work is dedicated to the LORD since science is simply the study of His creation;

To my wife, for her continuous support;

And to my children, who provide endless laughter in our home.

EPIGRAPH

The fear of the LORD is the beginning of knowledge;

Fools despise wisdom and instruction.

Proverbs 1:7

TABLE OF CONTENTS

LIST OF SYMBOLS AND ABBREVIATIONS

Angstrom	Å
Celsius	C
Channel Length	L
Channel width	W
Chemical Field Effect Transistor	chemFET
Cobalt phthalocyanine	CoPc
Copper phthalocyanine	CuPc
Current	I
Current-Voltage	I-V
Data acquisition system	DAQ
Derivative gain	K_d
Dimethyl methylphosphonate	DMMP
Direct Current	DC
Di-tert-Butyl Peroxide	DTBP
Drain Current	I_d
Drain Voltage	V_{ds}
Dual in-line package	DIP
Field Effect Transistor	FET
Gate Voltage	V_g
Gold	Au
Hertz	Hz
Hydrogen Peroxide	H_2O_2
Infrared	IR
Integral	I
Integral gain	K_i
Manipulated Variable	MV
Mass Flow Controller	MFC
Metal free phthalocyanine	H_2Pc
Metal Oxide semiconductor Field Effect Tranisitor	MOSFET
Metal-phthalocyanine	MPc

Millisecond	msec
millivolt	mV
Mobility	μ
Nanometer	Nm
Nitrogen Dioxide or Nitric Oxide	NO_x
Organic Semiconductro	OSC
Organic Thin Film Transistor	OTFT
Oxide captacitance	C_{ox}
Oxygen	O_2
Parts per million	PPM
Personal Computer	PC
Phthalocyanine	Pc
Printed circuit board	PCB
Process Variable	PV
Proportional	P
Proportional gain	K_p
Proportional-Integral-Derivative	PID
Pyrolytic Boron Nitride	PBN
Scanning Tunneling Microscopy	STM
Set Point	SP
Silicon	Si
Silicon Carbide	SiC
Silicon Dioxide	SiO_2
standard cubic centimeters per minute	sccm
Threshold Voltage	V_{th}
Titaninum	Ti
triacetone triperoxide	TATP
Ultra High Vaccum	UHV
Volts	V
Water	H_2O

LIST OF FIGURES

Chapter 1

Chapter 2

Chapter 3

ACKNOWLEDGEMENTS

I would like to thank my advisor, Professor Andy Kummel, and his close collaborator, Professor Bill Trogler for their guidance and instruction. I have benefited immeasurably from the experiences gained while a member of the Kummel Research Group.

I would also like to acknowledge and thank the United States Air Force who sponsored my assignment to graduate school. The Air Force Institute of Technology's Civilian Institution (AFIT-CI) program is an invaluable opportunity for Air Force officers to learn and develop the skills necessary for the future defense of our nation. Work covered this thesis was also funded by the Air Force Office of Scientific Research (AFOSR) Multidisciplinary Research Program of the University Research Initiative (MURI) grant.

The best laboratory experiences were gained not from scientific instruments, but from the members of the Kummel Lab. I would like to acknowledge Dr. Sangyeob Lee, and Jun Park for their expert STM advice and the images provided in Chapter 3. I would also like to acknowledge Tobin Kaufman-Osborn, Wil Melitz, Tyler Kent, David Martin, Dr. Joon Lee, Dr. Jian Shen, Dr. Jon Clemens, Dr. Sarah Bishop, and Dr. Evgueni Chagarov for their friendship and advice. I would especially like to thank Jim Royer, my lab partner, for the expert instruction he provided me during my studies.

Finally and most importantly, I would like to thank my God and my family. I believe God created the universe and everything in, what better way to learn about Him than trying to reverse engineer the science surrounding us

that He created. My wife Rozlyn has been a great support to me during my 18 month assignment. She bore me many a great laugh and two beautiful children, Annika and Gunner, both of which were born during my graduate program and provided me with plenty of extra “home work”.

VITA

2001-Present	United States Air Force
2005	Bachelor of Science, United States Air Force Academy
2011	Master of Science, University of California, San Diego

ABSTRACT OF THE THESIS

Mechanisms of Peroxide Sensing using Phthalocyanine Organic Thin Film Transistor Arrays

by

Erik Dennis Kappe

Master of Science in Chemistry

University of California, San Diego, 2011

Professor Andrew Kummel, Chair

Detection of gas phase hydrogen peroxide (H_2O_2) has growing importance in the security and defenses industries. Hydrogen peroxide based explosives are increasingly popular with terrorists as they are simple to synthesize from common materials. Triacetone triperoxide, a common hydrogen peroxide based explosive, can be detected by its release of hydrogen peroxide vapor upon exposure to UV light. A selective peroxide vapor detection method is demonstrated utilizing metal phthalocyanine (MPc) thin film transistors (chemFETs) which obviated the need for a detection array. The selective detection of vapor phase H_2O_2 on a single sensor element is demonstrated by recording on-current, mobility, and threshold voltage in MPc chemFETs. Doses of H_2O_2 cause an irreversible threshold voltage shift not evident with the non-oxidizing common background analytes such water and di-methyl methylphosphonate (DMMP). Furthermore, the V_{th} shift responds linearly to the dose time for exposure times of 1, 5, and 20 minutes, which permits dosiometric sensing analysis. ChemFET vapor detection of di-tert-butyl peroxide is also reported with varying shifts in V_{th} based on the metal center of the phthalocyanine film. This analysis permits a novel approach to selective H_2O_2 detection which is fundamentally different and potentially more selective than prior H_2O_2 detection methods.

1. Chapter 1: Organic Thin Film Transistors and Their Characterization by LabVIEW

1.1. Organic Thin Film Transistors (OTFTs)

1.1.1. Background

OTFTs are a type of thin film field-effect device with an organic thin film acting as the active semiconductor layer. The films in this study are composed of the organic semiconductor small molecule Phthalocyanine (Pc), either the metalated Pc (MPc) or the metal-free Pc (H_2Pc) as seen in

Figure 1.1. Pcs have nearly the longest history of use as organic semiconductors, and their field effect properties have been studied since the 1970s [1-2].

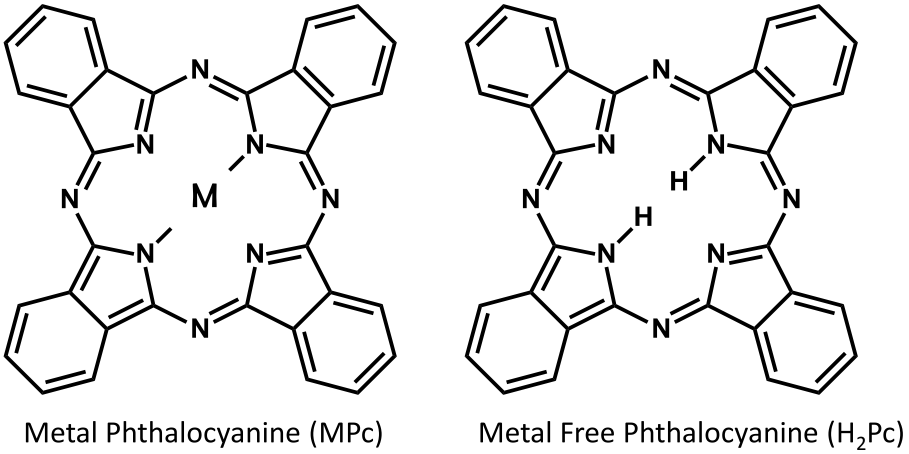

Figure 1.1: Molecular diagram of metal and metal free Phthalocyanine

1.1.2. Structure and Fabrication

A schematic cross-section of a typical OTFT device structure is presented in Figure 1.2.

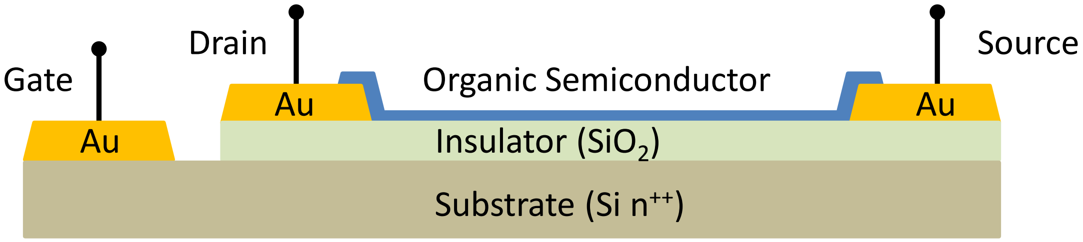

Figure 1.2: Schematic cross-section of a bottom contact OTFT

The device consists of two electrical contacts (source and drain) to the organic semiconductor (OSC) film, which is separated from a third electrode (gate) by an insulator material. These devices contain a 100nm dielectric layer of SiO_2.

Typically, source/drain contacts are deposited by electron-beam deposition using high work-function metals such as gold (Au) and patterned by standard lift-off lithography approaches. The contacts are composed of fifty pairs of interdigitated electrodes with a channel length of 5 μm and a channel width of 10 cm, Figure 1.3. Copper, cobalt or metal free phthalocyanine is deposited over the source/drain contacts as well as the insulator gate and acts as the organic semiconductor channel.

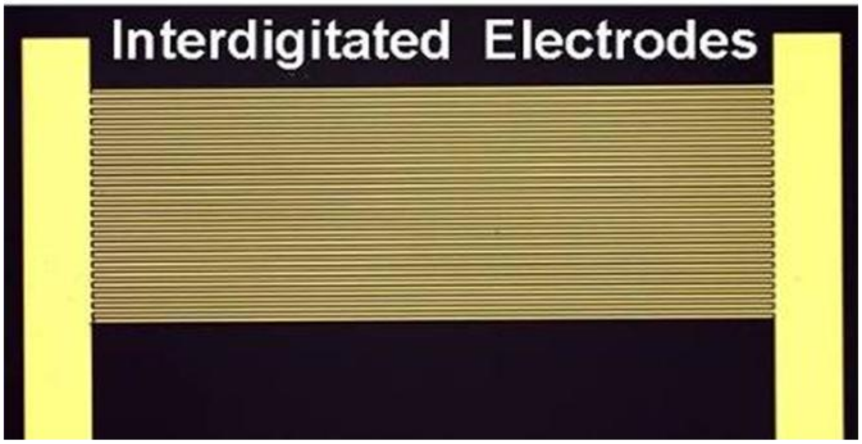

Figure 1.3: Interdigitated Au electrodes patterned by photolithography

There are a number of different methods for depositing organic thin films. Films can be created by solution-processed deposition such as spin-coating, ink-jet printing or roll-to-roll processing [3-4]. Solution-processed films are processed at low cost but film uniformity and controlling film microstructure can be challenging. OTFTs can also be created by the Langmuir-Blodgett technique[5-6]; however, this process is limited to amphiphilic molecules that have both polar and non-polar portions. Phthalocyanine films studied in this report were created by organic molecular beam deposition (OMBD)[7] . OMBD films can be deposited with good accuracy, but OMBD requires high vacuum or ultra-high vacuum (UHV) conditions for deposition. In this study, the UHV chamber is maintained at a base pressure of $2x10^{-10}$ Torr, Figure 1.4. UHV chambers are costly to maintain and yield low production quantities. Phthalocyanine is deposited by OMBD by evaporating Pc from a low temperature effusion cell at temperatures between 325°C and 365°C while the substrates maintained at room temperature. Deposition rates are between 0.5 and 1 Å/s.

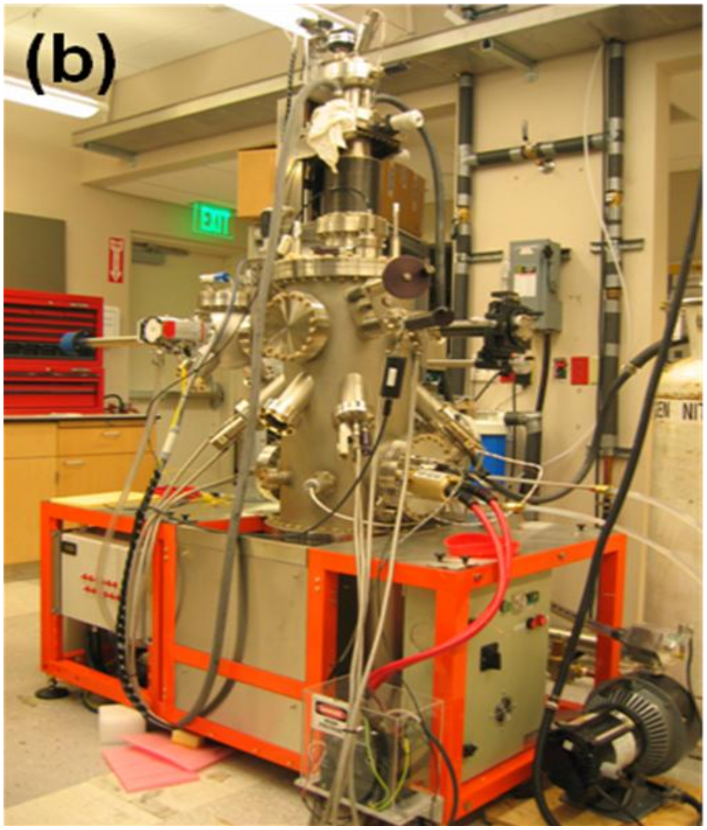

Figure 1.4: UHV Chamber used for evaporating Phthalocyanine onto substrates

1.1.3. Operation and Characterization

Transistor devices can be characterized by their threshold voltage (V_{th}), mobility (μ), and on/off ratio. In OTFT the source contact is connected to ground while a voltage is applied to the drain contact. The ability for current to pass through the organic from source to drain is controlled by the bias applied to the gate electrode. An organic semiconductor that contains positively charged dopants is called a p-type semiconductor. With p-type organic semiconductors, a negative voltage applied to the gate draws positive charges or "holes" from the bulk of the material to the surface of the insulator. As these "holes" accumulate, a channel of positive charge forms permitting electrons to flow through this conduction channel. At this point the

OTFT is considered to be in accumulation mode. The device is considered "turned on" when the conduction through the channel or 2D region dominates over the conduction of the bulk material or 3D.[8] Conversely, a positive voltage applied to the gate pushes the positive charge away from the insulator surface. This is known as depletion mode and conduction through the bulk material dominates, at this time the device is considered turned off.

In traditional MOSFETs, the threshold voltage is the gate voltage at which an inversion layer forms at the interface. Threshold voltage is measured in volts. Similar to accumulation mode, an inversion layer is a region close to the insulation layer in which the electronic field from the applied gate voltage causes a buildup of charge forming a conducting channel. In the case of MOSFETS, the p-type semiconductor becomes n-type or vice versa. Since the p or n types invert, it is known as the inversion layer. OTFTs do not form inversion layers, but channels do form in which conductivity through the film is several orders of magnitude higher than conductivity through the bulk material. OTFT devices operate in the accumulation regime since there is no depletion region to isolate the device from substrate.[9]

Mobility in a transistor is defined as the speed of charge carriers through the semiconductor in response to an electric field. Charges move more readily with a higher mobility, the units of mobility are $cm^2V^{-1}s^{-1}$.

OTFTs typically have uncompensated charge in the semiconductor due to unintentional doping by atmospheric contaminants or impurities. For phthalocyanine OTFTs, molecular oxygen (O_2) and atmospheric oxidants act as p-type dopants which oxidize the film causing uncompensated electron deficiencies (holes). [10-11] Therefore, the uncompensated dopants shift the threshold voltage to positive values, implying that charge can conduct through the film even at zero gate bias ($V_g = 0$ V). Therefore, when $V_g < V_{th}$, the device is considered on. When $V_g > V_{th}$, the uncompensated holes are depleted by the gate and the device is considered off. This is similar to traditional MOSFETs where the device is considered off at $V_g = 0$V if there is no fixed charge. The ratio in current through the device from these two states is the on/off ratio. Low off currents for OTFTs requires use of organic semiconductors which are minimally affected by atmospheric components.[12]

When these different parameters are combined, transistors become multiparametric devices. To extract device parameters, the current voltages (I-V) relationships of devices must be analyzed.

1.1.4. Current-Voltage (I-V) Curves

Typical current-voltage (I-V) output data for a phthalocyanine OTFT is presented in Figure 1.5. The drain current (I_d) is recorded for drain voltages (V_{ds}) between 0V and -10V for a series of fixed gate voltages (V_g). The OTFT I-V exhibit the same linear and saturation behavior observed in typical MOSFET devices.

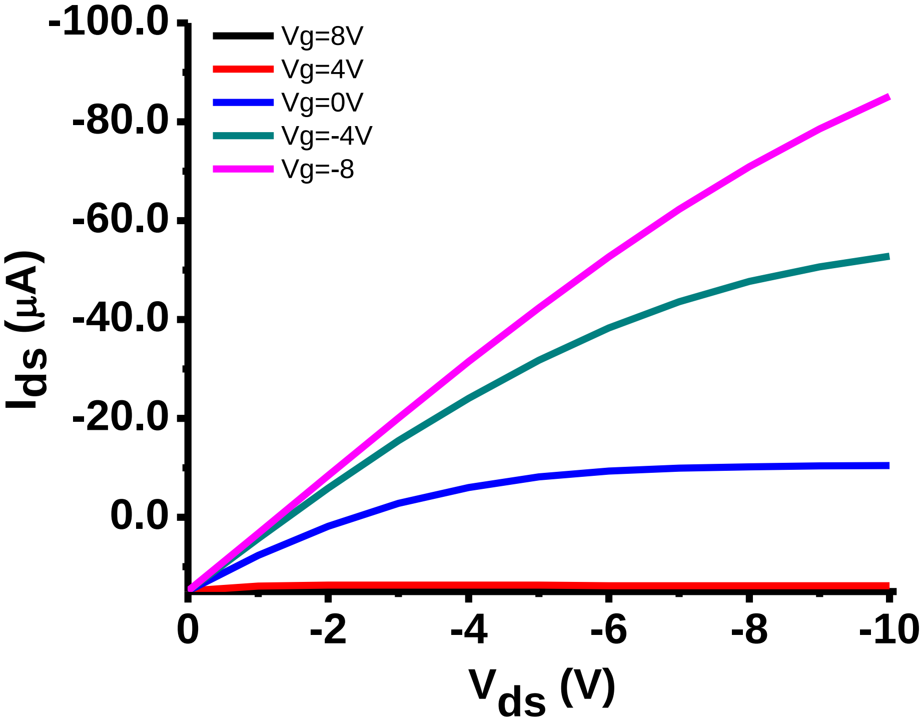

Figure 1.5: Standard current-voltage (I-V) output data

Reasonable turn off behavior indicated by low current is seen at +8V and +4V, but note the threshold voltage is not zero since there is high output current for V_g = 0V. At negative gate voltages, the current increases with decreasing gate voltage as expected.

While output I-V curves are created by fixing the gate and sweeping the drain voltage, transfer curves are created by fixing the drain voltage and sweeping the gate voltage. Typical phthalocyanine OTFT transfer data (I_d vs. V_g) are presented in Figure 1.6; note, this is a different device from Figure 1.5. Transfer data are useful for extracting the device properties such as V_{th} and mobility.

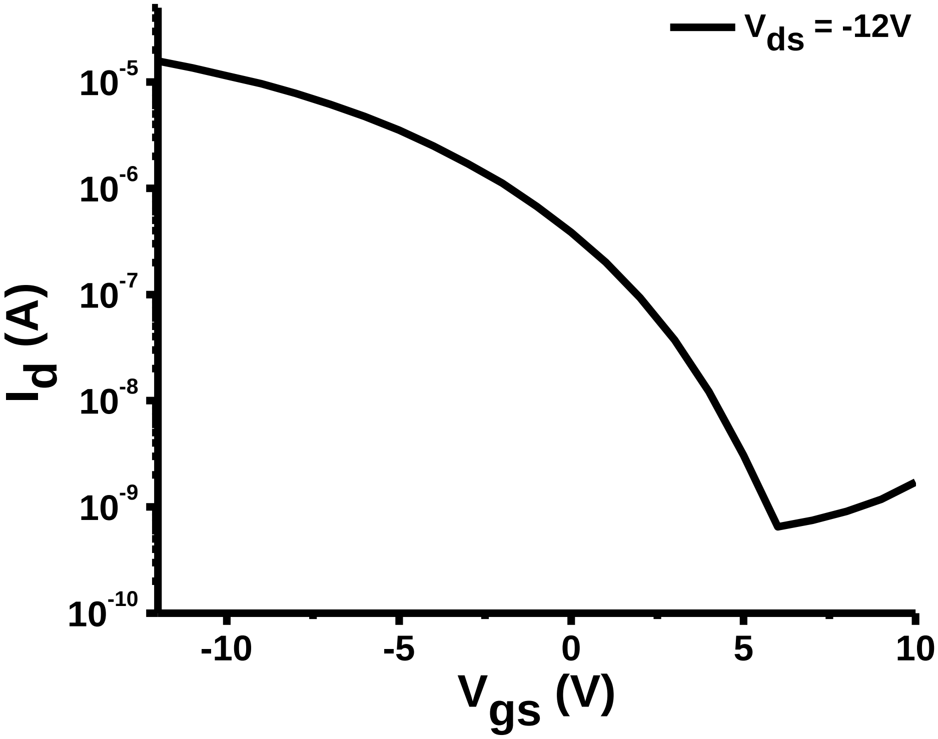

Figure 1.6: Typical phthalocyanine OTFT transfer data

To extract the values, a drain voltage of -12V is applied while the gate voltage is swept from +10V to -12V. The transfer data for Figure 1.6 is representative of an OTFT operating in the saturation regime, where the drain current is modeled by Equation (1-1) where *W* and *L* are channel width and length respectively, C_{ox} is the capacitance of the gate dielectric. By by plotting the square root of the drain current verses V_g , other transistor properties can be calculated[13].

$$I_D(sat) = \frac{W\mu C_{ox}}{2L}(V_{GS} - V_{th})^2 \tag{1-1}$$

By taking the square root of both sides, the equation can be rewritten in simplified form for plotting as seen in equation (1-2).

$$\sqrt{I_D(sat)} = \sqrt{\frac{W\mu C_{ox}}{2L}}(V_{GS} - V_{th}) \qquad (1\text{-}2)$$

Using this equation, the transfer curve can be plotted as seen in Figure 1.7 and mobility and threshold voltage can be extracted from the plot. A trend line plotted on the linear portion of the curve yields threshold voltage as the X-axis intercept. The slope of that same trend line contains mobility as shown in Equation (1-3).

$$Slope = \sqrt{\frac{W\mu C_{ox}}{2L}} \qquad (1\text{-}3)$$

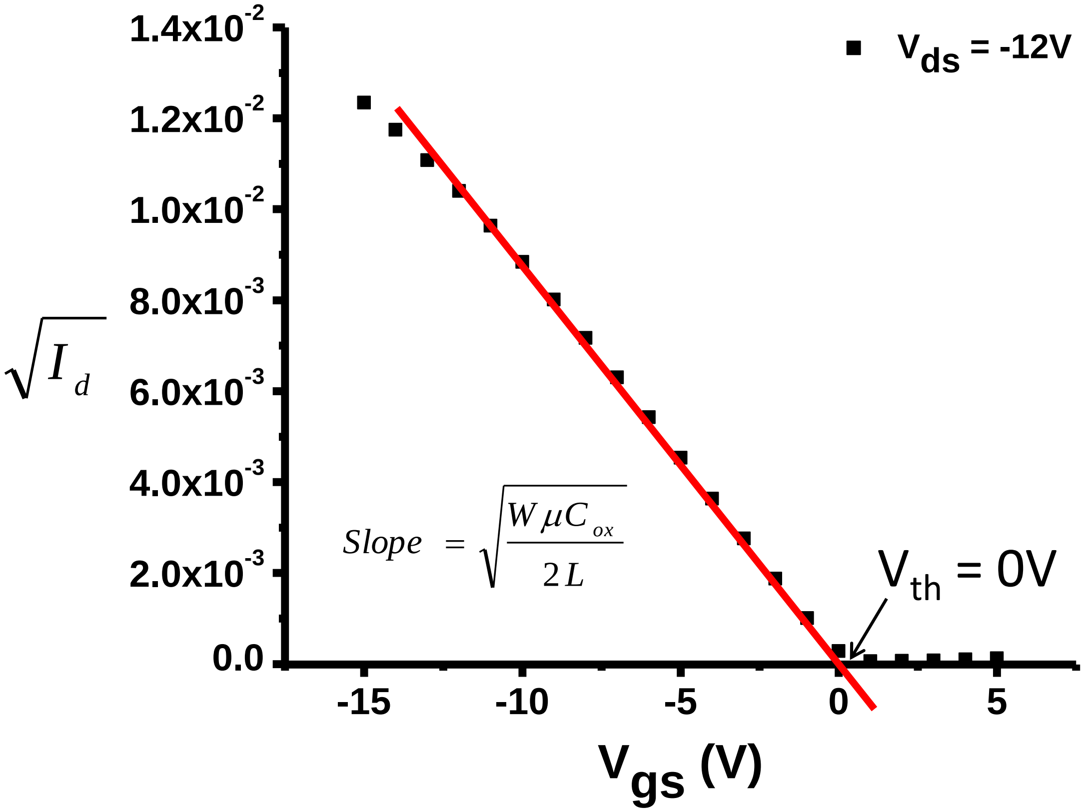

Figure 1.7: Square root of I_d vs. V_g, slope of the curve yields mobility while the crossing of the X-axis yields threshold voltage (V_{th})

The OTFT multiparametric analysis described above is employed with the data collection system described below.

1.2. Characterization Processes

1.2.1. Data Acquisition

Most laboratories require a data acquisition system (DAQ) in order to measure and record their experiments. For these experiments employed a National Instruments NI PXI-6259 M-Series Multifunction DAQ. This DAQ is a 32 channel, 16 bit DAQ capable of taking measurements at 1MS/s in the -10V to +10V range. It also has four 16 bit analog output channels outputs -10V to 10V. The input range is set in the -100mV to 100mV range.

After a thin film of Pc has been deposited by OMBD, chips are wire bonded with a West Bond Wedge Wire Bonder to a ceramic dual-inline package (DIP) from Spectrum Semiconductor Materials Inc, Figure 1.8.

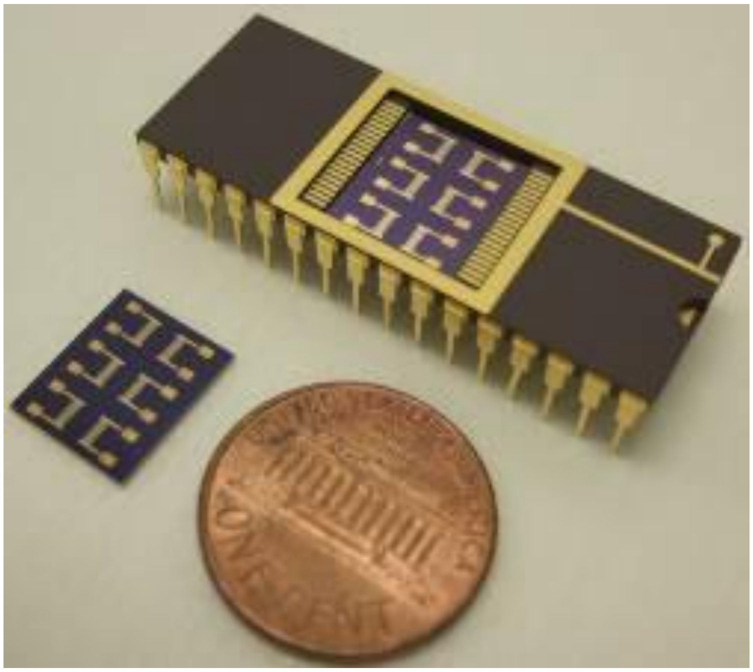

Figure 1.8: OTFT wafer containing 6 devices on left, wafer mounted in ceramic chip mount on right

The completed OTFT is inserted into a custom built printed circuit board, Figure 1.9, which is placed inside an air-tight, optically isolated test chamber connected to the DAQ.

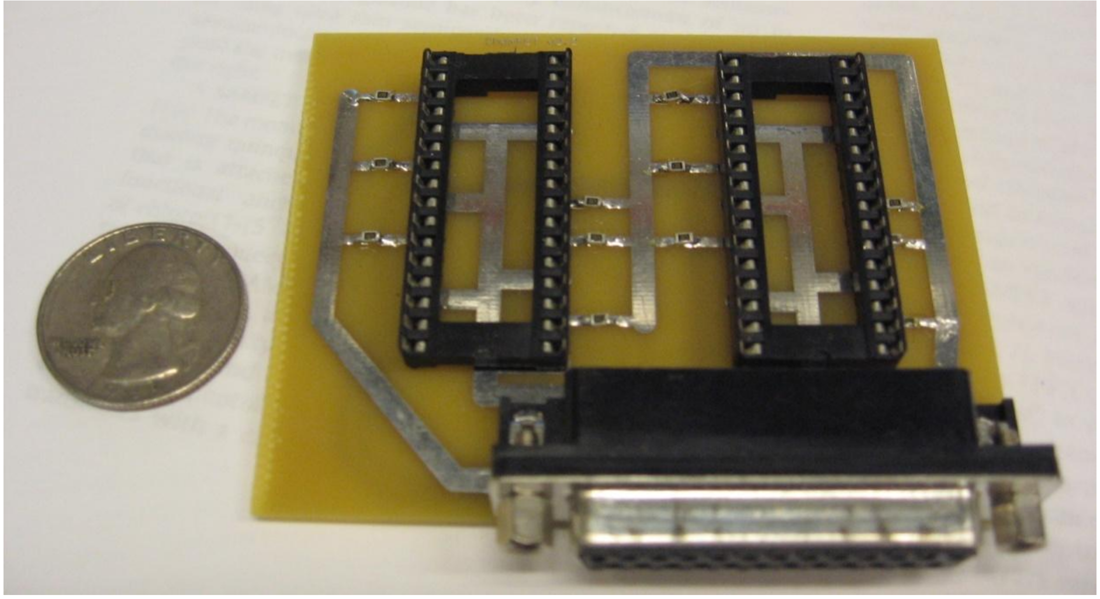

Figure 1.9: Picture of PCB, in-series resistors are visible. Coin for scale

The PCB adds an in-series resistor to the circuit. By measuring the voltage drop across the resistor with the DAQ, the current through the OTFT can be indirectly determined. Resistor values should be less than 1/1000th of the OTFT resistance. Figure 1.10 is the circuit diagram for measurement of an OTFT.

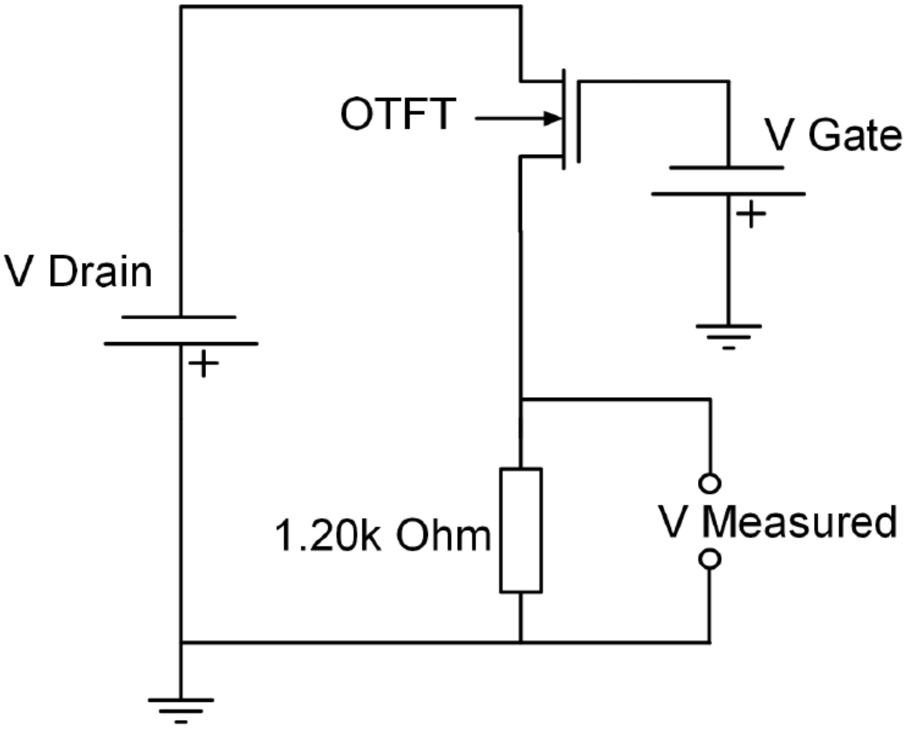

Figure 1.10: Circuit diagram for OTFT characterization, DAQ measures voltage drop cross the 1.20k Ω resistor at V measured.

Another method to measure the current through the device is with use of an op-amp.[14] The in-line resistor was chosen for a simpler design. Each PCB can hold two ceramic chips for a total of 12 OTFT sensors. Sensors can be any array of different metal or metal-free Pcs.

Dividing the measured voltage drop across the resistor by the known value of the resistor, current through each resistor is calculated using Ohm's Law, equation (1-4).

$$I = \frac{V}{R} \tag{1-4}$$

The calculated current is the same value of current through the OTFT due to Kirchhoff's current law.

1.2.2. Data Processing and Verification

A custom built National Instruments LabVIEW 2010 program controls data acquisition. LabVIEW employs a visual programming language geared towards laboratory applications. The LabVIEW program uses the DAQ to acquire the data, and subsequently processes, displays, analyzes, and stores the data.

Each OTFT is isolated on a single channel. IV curve data are generated by measuring the voltage drop across the in series resistor at each condition of V_g and V_{ds}. The LabVIEW program collects data at 80k samples per second. Steps of the IV sweep run at 10 Hertz; accordingly, the DAQ takes 8000 samples at each I-V sweep step. OTFTs have a turn on time of approximately 1 msec to allow the I_d to stabilize. To avoid collecting data during the OTFT settle period, the first 20% of the data points are discarded, reducing each sample size to 6400 points per step of each I-V sweep. These 6400 points are averaged to generate a single I_d point. Multiple I_d points generate an I_d verses V_g curve for further analysis. Standard deviation calculated for the 6400 points gives a general estimate of the electrical noise of the system. Values for the standard deviation are typically between 60-75 μV, mainly attributed to the DAQ which has a minimum voltage range accuracy of 52μV.

After acquisition, the baseline DC offset generated by the DAQ is subtracted from the measured values. To obtain the DC offset, the DAQ runs 0V on all outputs. The residual voltage measured on each channel constitutes the DC offset of the DAQ. The DC offset can change from run to run; therefore, it is updated periodically. The offset is measured repeatedly at any desired time interval. Each measured point is added to a moving average filter of the 5 last measured values.

After filtering and adjusting for DC offset, values for I_d are passed to an array containing all previous values. This array has two portions, a raw value portion and a relative percentage changed value portion calculated by the following equation (1-5).

$$\frac{I - I_\circ}{I_\circ} \times 100\ \% \qquad (1\text{-}5)$$

The array of run data are then plotted against time in an X-Y plot where it is updated real-time as the program runs.

Previous experiments measured only I_d at fixed V_g while passes were pulsed above the OTFTs; therefore, in these previous experiments the OTFT operated only as “enhanced” Chemiresistors.[10, 15-17]. Using programming, data analysis completed on the I_d allows the extraction of the threshold voltage (V_{th}) and the mobility (μ) from the I-V data as a function of time.

Extraction uses a data set where V_{ds} is held constant and V_g is swept from - V_{ds} to $+V_{ds}$. Using equation (1-2) data are plotted as Equation (1-6).

$$\sqrt{(I_{SD})_{sat}} = f(V_{GS}) \qquad (1\text{-}6)$$

LabVIEW accomplishes this by passing the points of the plot into a subroutine that can extract the slope from any portion of the curve. User inputs define which portion of the curve is employed to extract the mobility data and in the case of a V_g sweep of 10v to -10V typically it is the measurement from V_g -10V to -6V. This region is chosen because it lies in the linear saturation region. Mobility, μ, equals the square of the slope times a constant. V_{th} is extrapolated from the intersection of the slope with the x-axis as discussed earlier. LabVIEW calculates I_{on}/I_{off} ratio by dividing the on current at -10V by the off current at +10V.

After processing and displaying the data, LabVIEW saves all measurements to preformatted spreadsheets for future reference.

1.2.3. Applications

Before any sensing run, each device must be analyzed to verify good transistor behavior. All 12 channels can be verified at once using the setup previous described. Figure 1.11 shows an example I-V output preformed before a run. Eleven other graphs are simultaneously generated by which the user can quickly analyze the transistor behavior of all channels.

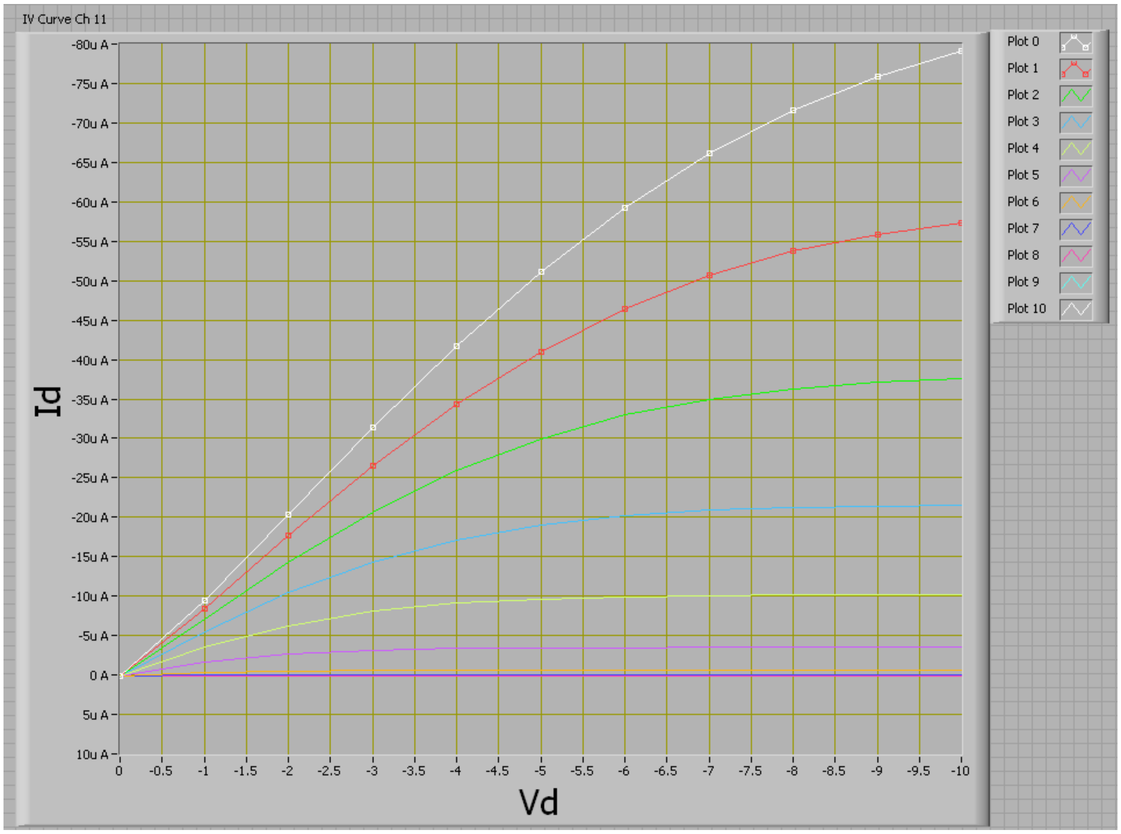

Figure 1.11: Sample I-V curve image gathered with OTFT analyzer.

After devices are verified as good transistors, sensing runs can be performed. During the run multiparametric data are gathered and can be viewed real time. Figure 1.12 displays a 3Pc sensor responding to doses of H_2O_2 and di-tert-Butyl peroxide. In this image V_{th}, μ, and I_d are displayed for 3 different sensors real time. Shifts in V_{th} are visible in the top row of each column while μ and I_d are visible in the bottom to rows.

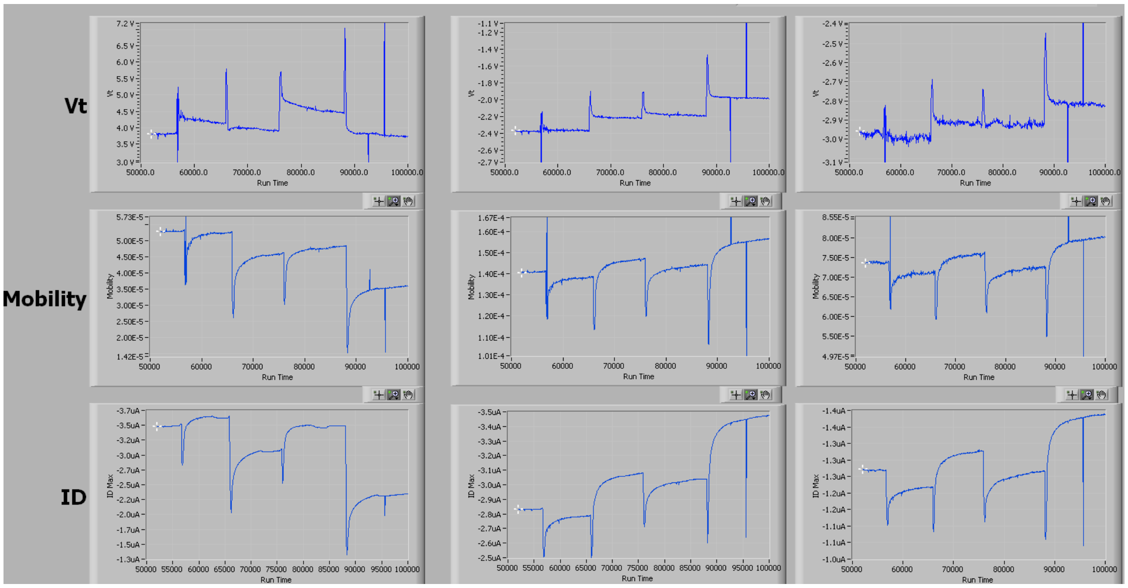

Figure 1.12: Example Multiparametric OTFT sensing data: CoPc (Left), CuPc (Middle), and H_2Pc (Right) sensing data for H_2O_2 and di-tert-Butyl peroxide doses.

1.3. Conclusion

Originally, only I_d was recorded; using the hardware and software described above, the transistor properties of I_d, μ, and V_{th}, are recorded as a function of time. This allows changes in the transistor properties to be measured in real time as analyte gasses pass above the OTFT. Through programming, a simple device measuring one OTFT property has been expanded to a multi-parameter OTFT analyzer.

1.4. References

1. Eley, D.D., *Phthalocyanines as Semiconductors.* Nature, 1948. **162**(4125): p. 819-819.

2. Barbe, D.F. and C.R. Westgate, *Surface state parameters of metal-free phthalocyanine single crystals.* Journal of Physics and Chemistry of Solids, 1970. **31**(12): p. 2679-2687.

3. Kagan, C.R., D.B. Mitzi, and C.D. Dimitrakopoulos, *Organic-Inorganic Hybrid Materials as Semiconducting Channels in Thin-Film Field-Effect Transistors.* Science, 1999. **286**(5441): p. 945-947.

4. Reese, C., et al., *Organic thin film transistors.* Materials Today, 2004. **7**(9): p. 20-27.

5. Petty, M.C., *Langmuir-blodgett films.* Endeavour, 1983. **7**(2): p. 65-69.

6. Barger, W.R., et al., *Derivatives of phthalocyanine prepared for deposition as thin films by the Langmuir-Blodgett technique.* Thin Solid Films, 1985. **133**(1-4): p. 197-206.

7. M. Bayliss, S., et al., *Thin film properties and surface morphology of metal free phthalocyanine films grown by organic molecular beam deposition.* Physical Chemistry Chemical Physics, 1999. **1**(15): p. 3673-3676.

8. Horowitz, G., *Organic Field-Effect Transistors.* Advanced Materials, 1998. **10**(5): p. 365-377.

9. Torsi, L. and A. Dodabalapur, *Organic Thin-Film Transistors as Plastic Analytical Sensors.* Analytical Chemistry, 2005. **77**(19): p. 380 A-387 A.

10. Yang, R.D., et al., *Analyte chemisorption and sensing on n- and p-channel copper phthalocyanine thin-film transistors.* The Journal of Chemical Physics, 2009. **130**(16): p. 164703.

11. Park, J., et al., *Ambient induced degradation and chemically activated recovery in copper phthalocyanine thin film transistors.* Journal of Applied Physics, 2009. **106**(3): p. 034505.

12. Saragi, T.P.I., T. Fuhrmann-Lieker, and J. Salbeck, *High ON/OFF ratio and stability of amorphous organic field-effect transistors based on spiro-linked compounds.* Synthetic Metals, 2005. **148**(3): p. 267-270.

13. Torsi, L., et al., *Multi-parameter gas sensors based on organic thin-film-transistors.* Sensors and Actuators B: Chemical, 2000. **67**(3): p. 312-316.

14. Das, A., et al., *Low cost, portable, fast multiparameter data acquisition system for organic transistor odour sensors.* Sensors and Actuators B: Chemical, 2009. **137**(2): p. 586-591.

15. Yang, R.D., et al., *Ultralow drift in organic thin-film transistor chemical sensors by pulsed gating.* Journal of Applied Physics, 2007. **102**(3): p. 034515.

16. Yang, R.D., et al., *Ultrathin organic transistors for chemical sensing.* Applied Physics Letters, 2007. **90**(26): p. 263506-3.

17. Park, J., et al., *Bilayer processing for an enhanced organic-electrode contact in ultrathin bottom contact organic transistors.* Applied Physics Letters, 2008. **92**(19): p. 193311.

2. Chapter 2: Selective detection of H_2O_2 vapor by means of Phthalocyanine OTFT V_{th} shifts

2.1. Abstract

A selective peroxide vapor detection method is demonstrated utilizing MPc thin film transistors (chemFETs) which obviated the need for a detection array. The selective detection of vapor phase H_2O_2 on a single sensor element is demonstrated by recording on-current, mobility, and threshold voltage in MPc chemFETs. Doses of H_2O_2 cause an irreversible threshold voltage shift not evident with the non-oxidizing common background analytes such water and di-methyl methylphosphonate (DMMP). Furthermore, the V_{th} shift responds linearly to the dose time for exposure times of 1, 5, and 20 minutes, which permits dosiometric sensing analysis. ChemFET vapor detection of di-tert-butyl peroxide is also reported with varying shifts in V_{th} based on metal center of the phthalocyanine film. This analysis permits a novel approach to selective H_2O_2 detection which is fundamentally different and potentially more selective than prior H_2O_2 detection methods.

2.2. Background

Detection of gas phase hydrogen peroxide (H_2O_2) has numerous applications in the medical and security fields. H_2O_2 in expired breath is a marker for acute respiratory failure[1] as well as acute airway inflammation [2]. In the security sector, hydrogen peroxide based explosives are increasingly popular with criminals and terrorists as they are simple to synthesize from common materials.[3] TATP, a hydrogen peroxide based explosive, is easily synthesized from common household chemicals: hydrogen peroxide, acetone, and sulfuric acid.[4] Hydrogen peroxide is very energetic and dangerous in pure form; at high concentrations, it is used as a monopropellant in satellites.[5] High concentration hydrogen peroxide can spontaneously decompose into water and oxygen with violent force. A hydrogen peroxide powered torpedo exploded accidentally with so much force that it sank the *Kursk*, a nuclear powered Russian cruise missile submarine.[6] Therefore, there is also a need to detect hydrogen peroxide for safety concerns.

Vapor phase hydrogen peroxide detection has been previously performed with several methods such as colorimetric sensor arrays [7], fluorescence detection [8], and amperometric sensors such as phthalocyanine chemiresistors [9]. Selective detection of H_2O_2 vapor has been demonstrated using differential responses from multiple metal-phthalocyanine (MPc) chemiresistors[9]. Selective MPc chemiresistor response is suggested to depend on the redox behavior of the central metal atom with H_2O_2. In this study, an alternative selective method is demonstrated utilizing MPc thin film transistors (chemFETs) which obviated the need for a detection array. In contrast to chemiresistors, chemFETs are capable of low signal drift, high sensitivity and fast recovery times [10-13]. Furthermore, chemFETs have multiple independent readout parameters including on-current, mobility (μ), and threshold voltage (V_{th}), which can be monitored for multiparametric sensing.[14-15] . The selective detection of vapor phase H_2O_2 on a single sensor element is demonstrated by recording on-current, mobility and threshold voltage in MPc chemFETs. Doses of H_2O_2 cause an irreversible threshold voltage shift which is not evident with the non-oxidizing common background analytes such water and di-methyl methylphosphonate (DMMP). Furthermore, the V_{th} shift responds linearly to the dose time for exposure times of 1, 5, and 20 minutes, which permits dosiometric sensing analysis. This analysis permits a novel approach to selective H_2O_2 detection which is fundamentally different and potentially more selective than prior H_2O_2 detection methods.

2.3. Experimental

2.3.1. Electrode Fabrication

Bottom-contact OTFTs were prepared by standard photolithography and a bilayer lift-off process. Electrodes were fabricated on n^+ silicon wafers with 100nm of thermally grown SiO_2.[16] 45 pairs of interdigitated electrodes were composed of a 5 nm Ti adhesion layer followed by a 45 nm gold layer to compose a 50 nm thick electrode. Six OTFT devices were fabricated on each chip with a channel length of 5μm and channel width of 10cm.

2.3.2. Organic Thin Film Deposition

CoPc (Aldrich, 97%), CuPc (Aldrich, 98%) and H_2Pc (Aldrich, 98%) were purified by multiple zone sublimations at 400°C and 10^{-5} Torr. Pc films were deposited by organic molecular beam deposition in a UHV chamber (base pressure 2×10^{-10} Torr). 4 monolayer (ML) films were deposited at 25°C at rates between 0.5 and 1 $Ås^{-1}$ with the aid of a quartz crystal microbalance. Film thicknesses were measured at 4ML as previously described.[17-18] CoPc, CuPc, and H_2Pc films were deposited on different devices on the same chip using shadow masks. This allowed each chip to contain six devices of three different films: 2 CoPc, 2 CuPc and 2 H_2Pc. An array of MPc ChemFETs on a single chip offers the advantage of testing of multiple Pc chemFETs concurrently although H_2O_2 detection is possible with a single device.

2.3.3. Device Measurement

Devices were optically isolated inside the testing chamber and held at 50˚C by means of a Haake F8 constant temperature bath connected by coolant lines. Measurements of the devices were recorded on a National Instruments PXI-6259 M-Series Multifunction DAQ and controlled by a custom built LabVIEW program. Current-voltage (*I-V*) data for the chemFETs were analyzed every 60 seconds by a gate voltage (V_g) sweep from +10V to -10V with the drain voltage (V_{ds}) held at -10V. Devices were stepped 1V every 100ms while V_{ds} was held at -10V for the duration of the gate sweep. V_g and V_{ds} were returned to 0V after complete of the sweep, OTFT were operated with a ~5% duty cycle. The threshold voltage and mobility for each device was recorded simultaneously using an automated LabVIEW program[19].

Chemical sensing experiments were conducted with a custom built computer controlled flow system. Using zero grade air carrier gas, flow through the testing chamber was kept at a constant 1000 standard cubic centimeters per minute (sccm) maintained by MKS Instruments Model 1479A mass flow controllers (MFCs). Carrier gas flow though impingement flasks full of analyte generated known concentrations of analytes. A Haake F8 controlled flask temperature at 25°C while MFCs regulated carrier gas flow rate. Analyte saturated carrier gas was further diluted by additional carrier gas to obtain desired concentrations. 4ML chemFET sensors were dosed with H_2O, H_2O_2, and DMMP at concentrations of 9378, 82ppm and 115ppm respectively. It is noted that some of the H_2O_2 may have reacted before flowing onto the sensors since calibrated dositubes showed that the H_2O_2 at the exit of the sensor flow system was only 25% of the concentration out of the bubbles; therefore, it is possible the sensitivities are 4x greater than reported.

For safety reasons 30% H_2O_2 in water (Fisher) was used, and the concentration of H_2O_2 in vapor phase over 30% H_2O_2 (aq) was derived from published data.[20-21]. At 25°C, the mole fraction of H_2O_2 in the vapor with respect to water above the solution is only 0.0114. Therefore, the vapor above a 30% solution of H_2O_2 is approximately 1 part H_2O_2 to 100 parts H_2O.[20] Any H_2O_2 dose is accompanied by a large water dose. H_2O_2 vapor was generated by running 300 sccm of zero grade air through 30% H_2O_2 in water (Fisher) and further diluted to 1000 sccm to generated 82 ppm of H_2O_2 vapor. Sensors were also dosed with Di-t-Butyl Peroxide (DTBP) purchased from Aldrich at 98%. vapor pressures from published data were used to generate concentrations of 12,838 ppm using the Clausius-Clapeyron equation.[22]

Results and Discussion

2.3.4. Transistor Characterization

Immediately after device fabrication, transistor properties were analyzed on an Agilent B1500 Semiconductor Device Analyzer. V_{th} and mobility were extracted according to equation (2-1) from the linear portion of the saturated region of the transfer curve.[23]

$$\sqrt{I_D(sat)} = \sqrt{\frac{W\mu C_{ox}}{2L}}\left(V_{GS} - V_{th}\right) \qquad (2\text{-}1)$$

Analyte effect on V_{th} has been demonstrated in previous work.[24-25] NO_x has caused V_{th} shifts in carbon nanotube sensors.[26]

2.4. Sensor Response to water and Hydrogen Peroxide

Figure 2.1 contains the sensing data for H_2O, H_2O_2 and DMMP on a 4ML H_2Pc sensor.

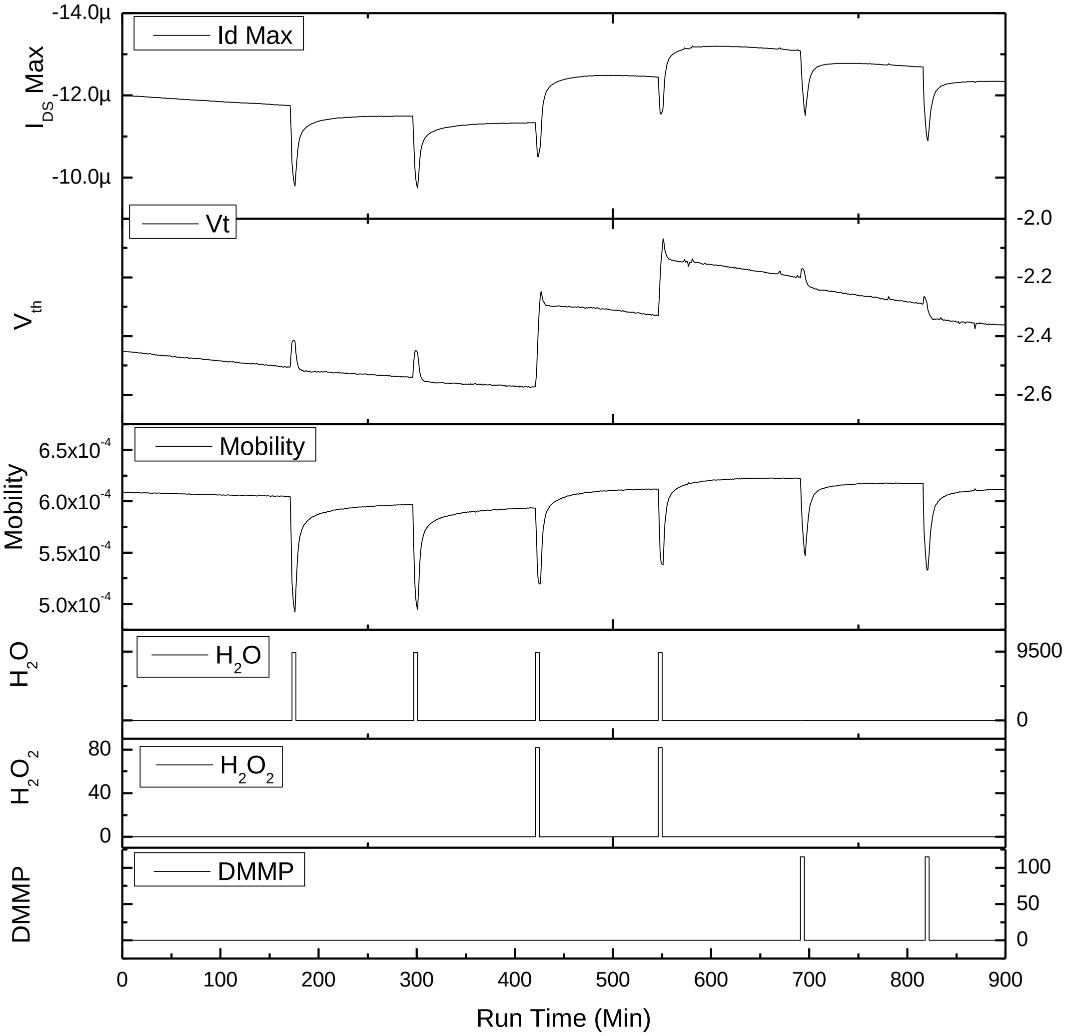

Figure 2.1: Six doses on ChemFET array H_2Pc data shown; 9378 ppm of water (doses 1 and 2), 82ppm of H_2O_2 in water (doses 3 and 4) and 115ppm of DMMP (doses 5 and 6). All doses were 5 minutes. Drain current decreases reversibly upon exposure to H_2O and DMMP; conversely, the drain current initially decreases upon exposure to H_2O_2/H_2O but then increases irreversibly. This transient is caused by the faster adsorption of H_2O than H_2O_2. While H_2O and DMMP cause reversible changes in output current, only H_2O_2 causes an irreversible change in output current. The automated I-V analysis shows that the H_2O, H_2O_2, and DMMP induce reversible decreases in mobility. Selectivity to H_2O_2 is present in the Automated I-V analysis of V_{th}. H_2O and DMMP cause transients in V_{th} while H_2O_2 (doses 3 and 4) induces an irreversible change in threshold voltage.

The dosing profile starts with water as a control. ChemFET sensors were dosed twice with water at 9378 ppm for 5 minutes. Pulses 1 and 2 in Figure 2.1 demonstrated the effect of pure water on H_2Pc chemFET. Water causes a reversible decrease in the magnitude of the output current. Using the automated transfer curve fitting model, mobility and V_{th} were extracted. H_2O caused a reversible decrease in mobility and a transient increase in the threshold voltage but no persistent shift in threshold voltage.[27] The observed V_{th} spike is most likely due to limitations of equation (2-1) during automated transfer curve fitting.

Pulses 3 and 4 in Figure 2.1 were 5 minutes doses of 82 ppm H_2O_2 accompanied by 9378 ppm of water. The H_2Pc chemFET sensor showed a nearly irreversible increase in output current with a small transient increase presumably from the H_2O_2 and the H_2O respectively. The automated I-V fitting program decomposed the changes in output current for these peroxide containing pulses to being mostly an irreversible increase in threshold voltage (presumably from H_2O_2) and a reversible decrease in mobility (presumably from H_2O). This demonstrates the selectivity of H_2O_2 to V_{th} by the effect of H_2O_2/H_2O pulses on V_{th}.

Finally pulses 5 and 6 in Figure 2.1 show the effects of 115 ppm DMMP for 5 minutes. DMMP causes a reversible decrease in output current. The automated fitting program models this change as a reversible decrease in mobility and a very small transient increase in the V_{th}.

Even though all three gasses gave indistinguishable changes in mobility, only the hydrogen peroxide induces a nearly irreversible change in output current and threshold voltage; this is the basis of the selective sensing.

Data for H_2Pc are shown in Figure 2.1, but CoPc and CuPc data not shown yielded similar V_{th} shifts and selectivity.

To remove the initial spikes in V_{th} and I_d max at the beginning of each H_2O_2 dose in Figure 2.1, counter dosing of water was performed. the chemFET sensors were stabilize with 9378 ppm of water prior to introduction of H_2O_2. During the H_2O_2 dose, the water background was removed to maintain the chamber at a constant 9378ppm. This counter dosing scheme kept the ppm of water constant throughout the introduction of H_2O_2, allowing the effects of H_2O_2 to be isolated from the water influence. Counter-dosing better reflects real world application of H_2O_2 sensors where atmospheric humidity would remain unchanged with the presence of H_2O_2.

Figure 2.2 contains counter-dosing data from an H_2Pc sensor. In Figure 2.2, 5 minute doses of 82 ppm H_2O_2 cause irreversible increases in I_d max without the initial transients seen in H_2O_2 dosing in Figure 2.1. Automated I-V analysis of V_{th} reveals irreversibly V_{th} increases to H_2O_2 with water counter dosing, eliminating the overshoot present in Figure 2.1. Extracted mobility reversibly increased in response to H_2O_2 dose whereas in the non-counter dosing experiment, dosing of H_2O_2 induced a reversible decrease in mobility. Counter dosing of H_2O_2 pulses with background water removes initial transients and spikes from output current and V_{th} shifts and causes a reversible increase rather than decrease in transistor mobility.

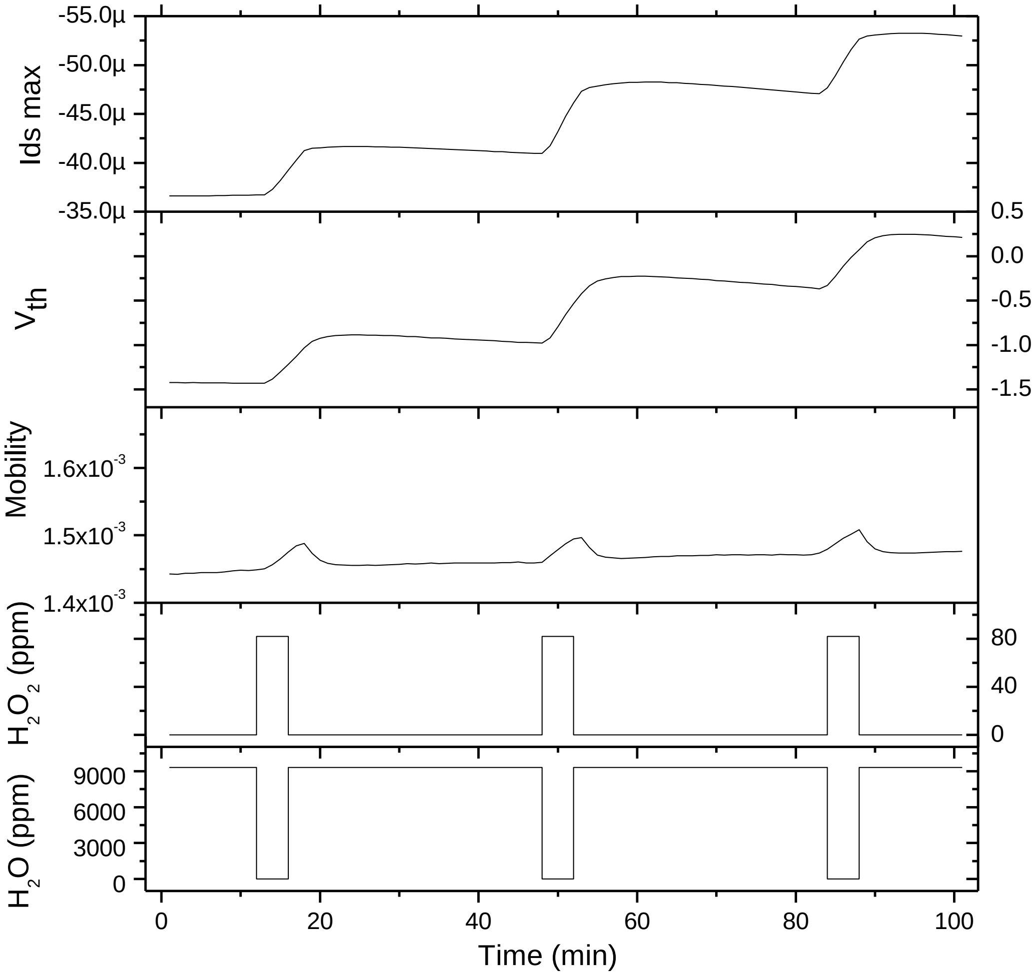

Figure 2.2: 5 minutes 82 ppm H_2O_2 doses in a constant water background of 9378 ppm throughout sensing run. The chemFET sensors were stabilize with 9378 ppm of water prior to introduction of H_2O_2. During the H_2O_2 dose, the water background was removed to maintain the chamber at a constant 9378ppm. H_2O_2 caused irreversible increases in I_d max without the initial transients seen in H_2O_2 dosing from Figure 2.1. Automated I-V analysis of V_{th} reveals irreversibly V_{th} increases to H_2O_2 with water counter dosing, eliminating the overshoot present in Figure 2.1. Extracted mobility reversibly increased in response to H_2O_2 dose whereas in non-counter dosing to H_2O_2 incited a reversible decrease in mobility. This counter dosing scheme kept the ppm of water constant throughout the introduction of H_2O_2, allowing the effects of H_2O_2 to be isolated from the water influence.

On a device level, there are two possible mechanisms for chemFET reaction to H_2O_2: (1) H_2O_2 as a strong oxidizer is introducing trapped charge into the film (2) H_2O_2 decomposes the phthalocyanine thin film increasing the trapped change in the film. Work by Bohrer et al. as seen in Figure 2.3 demonstrated that H_2O_2 decomposes FePc.[28]

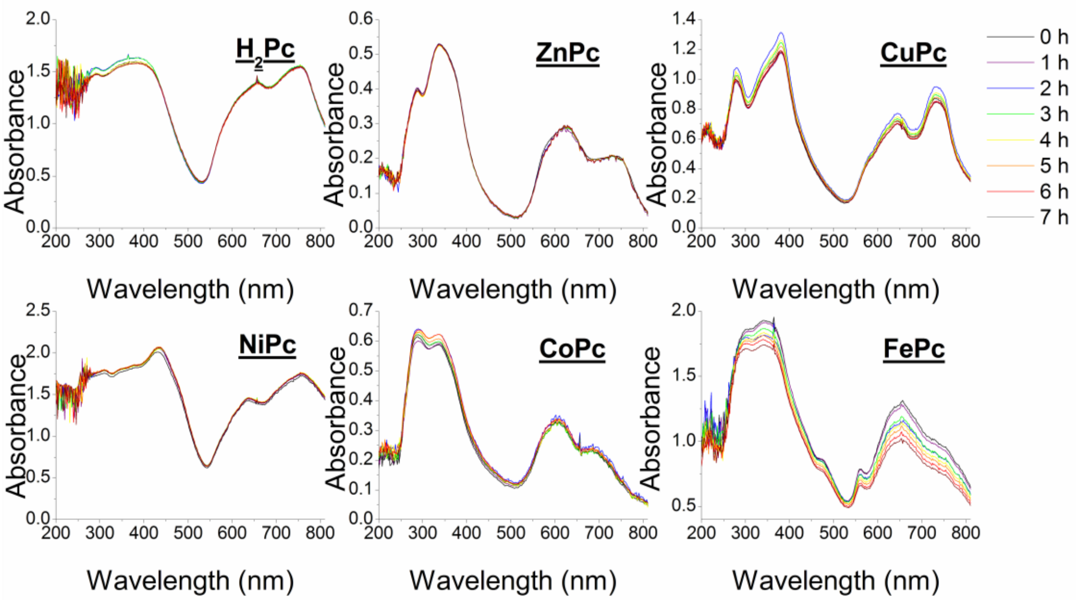

Figure 2.3: UV/Vis absorption spectra of thin evaporated films of MPcs on glass. The films were exposed to vapors of 5% H_2O_2 (aq) solution (~24 ppm H_2O_2) at room temperature and spectra were taken hourly. FePc, CuPc and CoPc show a marked decrease in intensity with H_2O_2 exposure. Image used from Bohrer et al. [28]

Trapped charge has been responsible for V_{th} shifts in other OTFTs, and the trapped charge mechanism may not be exclusive to peroxides. [15] Phthalocyanine films are oxidized by other strong oxidizers such as NO_x resulting in V_{th} shifts [29] In constant, multiple common analytes including alcohols, aromatics, alkanes, phosphonates, ketones, aldehydes are known to have reversible absorption on MPcs without irreversible changes in trapped charge.[17] Therefore, the peroxide fixed charge effect can be employed to develop a very selective sensor.

The trapped charge mechanism allows very sensitive detection of peroxide since the response is an integral of time, i.e. dosiometric. Typically, chemFET sensors are only responsive to concentration of the analyte, not dose volume.[30] For a given analyte concentration, most analytes give a constant response in time after the surface concentration reaches equilibrium. H_2O_2 cause shifts in threshold voltage dosiometrically, longer doses produce larger shifts in V_{th} shift. 82 ppm of H_2O_2 dosed for 1, 5, and 20 minutes caused increasing shifts in V_{th} as shown in Figure 2.4. In Figure 2.4, the counter dosing method was not employed so transients in output current, V_{th}, and mobility are present.

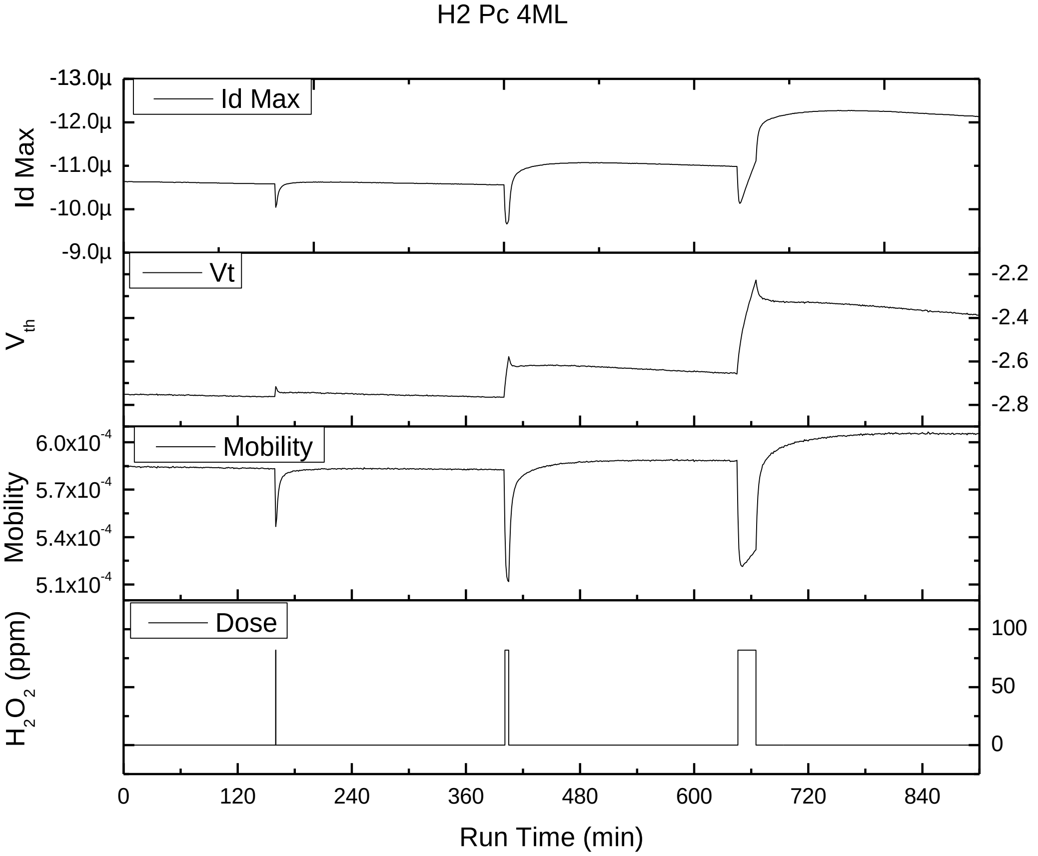

Figure 2.4: H_2O_2 Dosiometric test on 4ML of H_2Pc: 82 ppm of H_2O_2 was dosed for 1, 5 and 20 minutes. Drain current responded as expected from Figure 2.1 but with dosiometric effects, longer doses yielded greater irreversible increased in the drain current. Current decrease transients occur due to the lack of counter dosing. Automated I-V analysis yields increasing irreversible increases in V_{th} according to longer H_2O_2 doses. Extracted mobility showed reversible decreases in mobility during H_2O_2 dose. Irreversible changes in output current and V_{th} scale with the dose length. The small transient changes in threshold voltage as well as the reversible changes in

mobility were likely due to the co-dosing with water since the water counter dosing method was not employed.

In, Figure 2.5, the change in V_{th} is plotted against H_2O_2 dose time from Figure 2.4. The magnitude of the V_{th} is linearly proportional to the dose length.

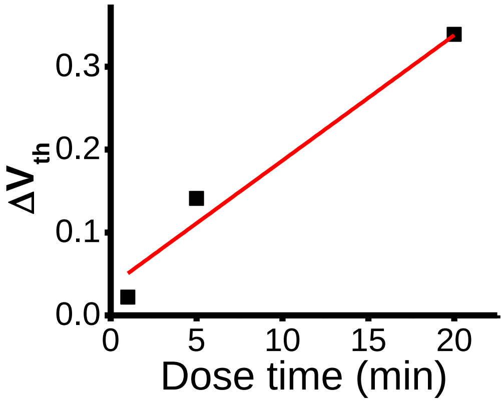

Figure 2.5: Shift in V_{th} verses H_2O_2 exposure time: These data are obtained from the V_{th} response in Figure 2.4 where a 4ML H_2Pc chemFET was dosed with 82 ppm of H_2O_2 for 1, 5 and 20 minutes, longer doses yield greater irreversible increased in the drain voltage. Automated I-V analysis showed irreversible changes in output current were induced by irreversible shifts in threshold voltages which scaled with the dose length.

This dosiometric response implies that low concentrations of H_2O_2 can be detected by sampling for extended periods of time. In theory, a 100 minute dose at 0.82 ppm would cause the same V_{th} shift as a 1 min dose at 82 ppm. Experimentally, it is difficult to maintain very low concentrations of H_2O_2 in the sensing chamber due to spontaneous decomposition of H_2O_2 into O_2 and water. With dosiometric responses, concentrations of 0.4 ppm should be detectable with 4ML H_2Pc chemFETs.

2.5. Sensor Response to Organic Peroxides

In addition to hydrogen peroxide, ChemFET sensors were dosed with organic peroxide, di-tert-butyl peroxide (DTBP) whose structure is shown in

Figure 2.6. These experiments investigated the differences in chemFET response to organic peroxides in contrast to hydrogen peroxide.

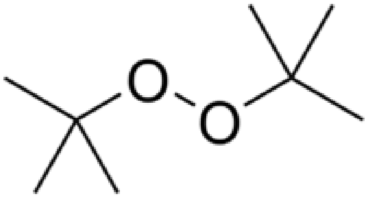

Figure 2.6: Di-tert-butyl Peroxide (DTBP), organic peroxide. The molecules share the weak O-O single bond with HOOH and therefore are expect to induce similar responses on chemFETs.

Figure 2.7 is the output current data from a comparative sensing run of DTBP and H_2O_2 on 3 different Pc films, CoPc, CuPc, and H_2Pc. Two doses of DTBP and two doses of H_2O_2 were employed.

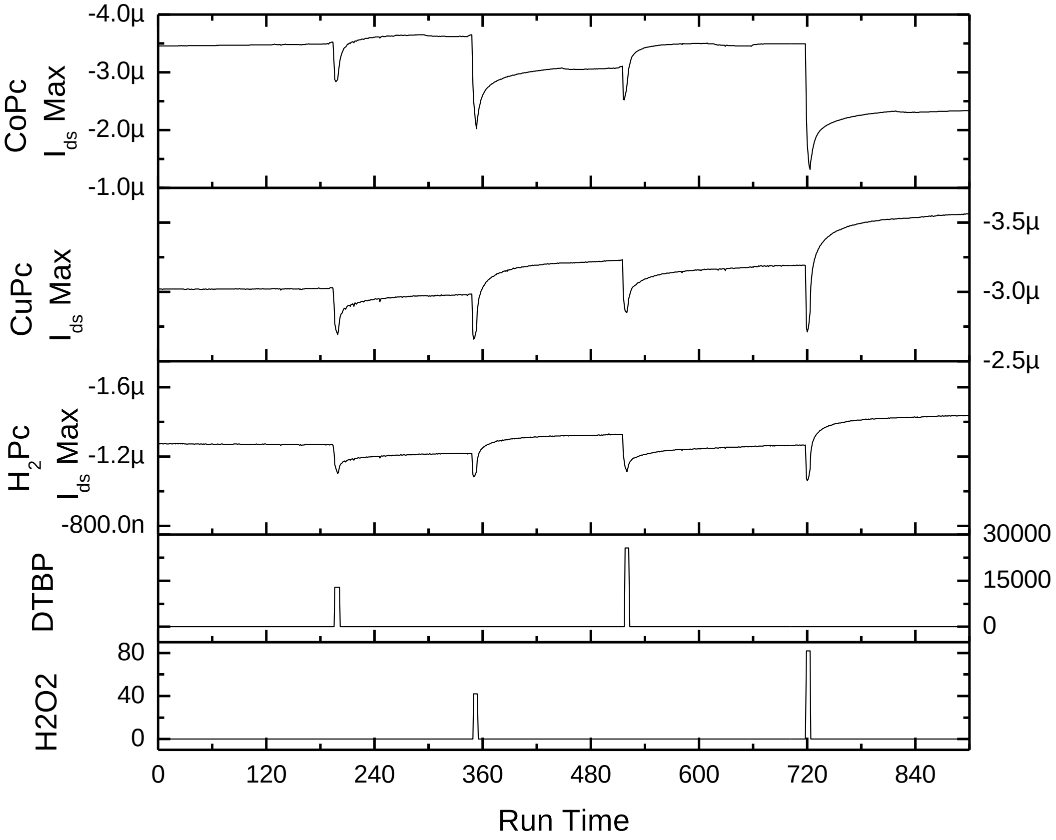

Figure 2.7: Drain current response to 5 minute DTBP and H_2O_2 doses. Pulse 1 dosed 12838 ppm DTBP, pulse 2 dosed 41 ppm H_2O_2, pulse 3 dosed 25676 ppm DTBP, pulse 4 dosed 82 ppm of H_2O_2. Doses 1 and 3 of DTBP caused a slight current increase in CoPc and a current decrease in CuPc and H_2Pc. Doses 2 and 4 of H_2O_2 caused a current decrease in CoPc and a current increase in CuPc and H_2Pc. Doses 3 and 4 were double the strength of doses 1 and 2 respectively, current response scaled accordingly.

Figure 2.7 demonstrates a chemFET array's drain current response to 5 minute DTBP and H_2O_2 doses. Pulse 1 dosed 12838 ppm DTBP, pulse 2 dosed 41 ppm H_2O_2, pulse 3 dosed 25676 ppm DTBP, and pulse 4 dosed 82 ppm of H_2O_2. Doses 1 and 3 of DTBP caused a slight irreversible current increase in CoPc and an irreversible current decrease in CuPc and H_2Pc. Doses 2 and 4 of H_2O_2 caused an irreversible current decrease in CoPc and an irreversible current increase in CuPc and H_2Pc. Doses 3 and 4 were double the strength of doses 1 and 2 respectively, current response scaled accordingly.

Current data from Figure 2.7 was analyzed by the automatic I-V curve analyzer to produce threshold voltage as displayed in Figure 2.8. Doses 1 and 3 of DTBP, shows no change in V_{th} of H_2Pc while CuPc had a ~.1V irreversible increase and CoPc had an irreversible ~.5V increase in V_{th}. CoPc is more responsive to DTBP than CuPc while H_2Pc is nearly unresponsive. This demonstrates that different phthalocyanine metal center have different sensitivity to organic peroxide.

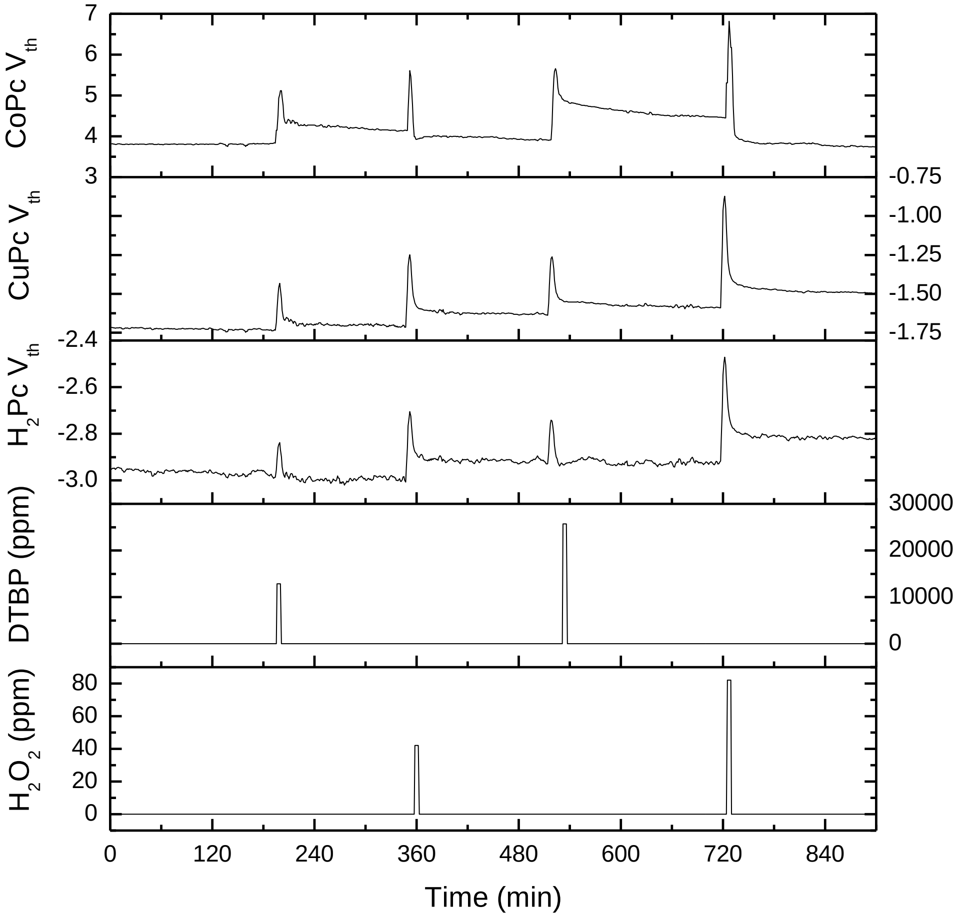

Figure 2.8: Di-t-Butyl peroxide (DTPB) and H_2O_2 doses on CoPc, CuPc and H_2Pc. Doses 1 and 3 are 12838 and 25676 ppm DTPB while doses 2 and 4 are 41 and 82 ppm hydrogen peroxide. All doses were 5 minutes long. Automated I-V analysis of the drain current from Figure 2.7 provided the changes V_{th} as a function of time. In response to DTPB, CoPc had an irreversible V_{th} increase of ~0.5V while CuPc had an irreversible increase of 0.1V. H_2Pc showed almost no shift in V_{th} in response to DTPB. As a control, H_2O_2 was also run at doses 2 and 4. CuPc and H_2Pc both showed an irreversible increase in V_{th} upon exposure to H_2O_2 while CoPc showed a decrease in V_{th}. This demonstrates that different phthalocyanine metal center have different sensitivity to organic peroxide.

V_{th} responses in Figure 2.8 imply that with DTBP, irrecoverable V_{th} shift may be dependent on the metal center of the phthalocyanine.

2.6. Conclusion

In this study, selectivity of detecting H_2O_2 has been obtained by monitoring V_{th} and mobility in addition to I_d. By monitoring V_{th} 100% selectivity to H_2O_2 from water and other analytes is possible. Furthermore, the system responds dosiometrically making high sensitivity possible. These sensors are more selective than chemiresistors and for H_2O_2 do not require an array for peroxide detection. ChemFETs have also demonstrated different sensitivities to DTBP based on the metal center of the phthalocyanine film.

2.7. References

1. Kietzmann, D., et al., Hydrogen peroxide in expired breath condensate of patients with acute respiratory failure and with ARDS. Intensive Care Medicine, 1993. **19**(2): p. 78-81.

2. Dohlman, A.W., H.R. Black, and J.A. Royall, Expired Breath Hydrogen-Peroxide Is a Marker of Acute Airway Inflammation in Pediatric-Patients with Asthma. American Review of Respiratory Disease, 1993. **148**(4): p. 955-960.

3. Wang, J., Electrochemical Sensing of Explosives. Electroanalysis, 2007. **19**(4): p. 415-423.

4. Burks, R. and D. Hage, Current trends in the detection of peroxide-based explosives. Analytical and Bioanalytical Chemistry, 2009. **395**(2): p. 301-313.

5. Darren, L.H. and et al., MEMS-based satellite micropropulsion via catalyzed hydrogen peroxide decomposition. Smart Materials and Structures, 2001. **10**(6): p. 1163.

6. Shteinberg, A.S., High-Temperature Decomposition and Thermal Explosion of Liquid Propellant Components: Hydrogen Peroxide and Hydrazine, in Fast Reactions in Energetic Materials. 2008, Springer Berlin Heidelberg. p. 173-198.

7. Lin, H. and K.S. Suslick, A Colorimetric Sensor Array for Detection of Triacetone Triperoxide Vapor. Journal of the American Chemical Society, 2010. **132**(44): p. 15519-15521.

8. Sanchez, J.C. and W.C. Trogler, Polymerization of a boronate-functionalized fluorophore by double transesterification: applications to fluorescence detection of hydrogen peroxide vapor. Journal of Materials Chemistry, 2008. **18**(42): p. 5134-5141.

9. Bohrer, F.I., et al., Selective Detection of Vapor Phase Hydrogen Peroxide with Phthalocyanine Chemiresistors. Journal of the American Chemical Society, 2008. **130**(12): p. 3712-3713.

10. Torsi, L., A. Dodabalapur, and H.E. Katz, An analytical model for short-channel organic thin-film transistors. Journal of Applied Physics, 1995. **78**(2): p. 1088-1093.

11. Yang, R.D., et al., Ultralow drift in organic thin-film transistor chemical sensors by pulsed gating. Journal of Applied Physics, 2007. **102**(3): p. 034515.

12. Yang, R.D., et al., Analyte chemisorption and sensing on n- and p-channel copper phthalocyanine thin-film transistors. The Journal of Chemical Physics, 2009. **130**(16): p. 164703.

13. Bouvet, M., Phthalocyanine-based field-effect transistors as gas sensors. Analytical and Bioanalytical Chemistry, 2006. **384**(2): p. 366-373.

14. Torsi, L., et al., Multi-parameter gas sensors based on organic thin-film-transistors. Sensors and Actuators B: Chemical, 2000. **67**(3): p. 312-316.

15. Torsi, L. and A. Dodabalapur, Organic Thin-Film Transistors as Plastic Analytical Sensors. Analytical Chemistry, 2005. **77**(19): p. 380 A-387 A.

16. Park, J., et al., Bilayer processing for an enhanced organic-electrode contact in ultrathin bottom contact organic transistors. Applied Physics Letters, 2008. **92**(19): p. 193311.

17. Bohrer, F.I., et al., Comparative Gas Sensing in Cobalt, Nickel, Copper, Zinc, and Metal-Free Phthalocyanine Chemiresistors. Journal of the American Chemical Society, 2008. **131**(2): p. 478-485.

18. Royer, J.E., et al. Mobility saturation in tapered edge bottom contact copper phthalocyanine thin film transistors. 2010: AVS.

19. Schroder, D.K., Semiconductor Material and Device Characterization. 1998, New York: Wiley.

20. Manatt, S.L. and M.R.R. Manatt, On the Analyses of Mixture Vapor Pressure Data: The Hydrogen Peroxide/Water System and Its Excess Thermodynamic Functions. Chemistry – A European Journal, 2004. **10**(24): p. 6540-6557.

21. Scatchard, G., G.M. Kavanagh, and L.B. Ticknor, Vapor-Liquid Equilibrium. VIII. Hydrogen Peroxide—Water Mixtures1. Journal of the American Chemical Society, 1952. **74**(15): p. 3715-3720.

22. Diogo, H.P., et al., Standard enthalpy of formation and enthalpy of vaporization of di-1,1-dimethylethyl peroxide: Re-evaluation of the standard enthalpy of formation of the di-1,1-dimethylethoxy radical. The Journal of Chemical Thermodynamics, 1995. **27**(6): p. 597-604.

23. Neamen, D., An Introduction to Semiconductor Devices. 1 ed. 2006, New York: McGraw-Hill, Inc. 720.

24. Crone, B., et al., Electronic sensing of vapors with organic transistors. Applied Physics Letters, 2001. **78**(15): p. 2229-2231.

25. Das, A., et al., Low cost, portable, fast multiparameter data acquisition system for organic transistor odour sensors. Sensors and Actuators B: Chemical, 2009. **137**(2): p. 586-591.

26. Qi, P., et al., Toward Large Arrays of Multiplex Functionalized Carbon Nanotube Sensors for Highly Sensitive and Selective Molecular Detection. Nano Letters, 2003. **3**(3): p. 347-351.

27. Belghachi, A. and R.A. Collins, Humidity response of phthalocyanine gas sensors. Journal of Physics D: Applied Physics, 1988. **21**(11): p. 1647.

28. Bohrer, F.I.a.C., C. N., Selective Vapor-Phase Detection of Peroxides with Chemiresistive Metal Phthalocyanine Nanofilms. Unpublished.

29. Park, J., et al., Ambient induced degradation and chemically activated recovery in copper phthalocyanine thin film transistors. Journal of Applied Physics, 2009. **106**(3): p. 034505.

30. Bohrer, F.I., et al., Gas Sensing Mechanism in Chemiresistive Cobalt and Metal-Free Phthalocyanine Thin Films. Journal of the American Chemical Society, 2007. **129**(17): p. 5640-5646.

3. CHAPTER 3: Surface Reconstruction via LabVIEW PID controlled annealing system

3.1. Background

Atomic resolution scanning tunneling microscopy (STM) requires minimal surface defects and surface roughness in the imaged surface.[1] One way of preparing such a surface is with heat treatment. Both single crystal gold (Au) and silicon (Si) samples have been prepared by computer controlled heat treatment profiles and have been imaged in ultra high vacuum (UHV) conditions. A LabVIEW program utilizing a proportional-integral-derivative (PID) feedback loop was developed and employed to control heat treatment of the samples prior to imaging. Si surfaces were prepared by “flashing” then annealing while the Au surface was prepared by annealing. With proper surface preparation, atomic resolution images of these surfaces are routinely obtained. These prepared surfaces are useful for imaging and study of the small molecule phthalocyanine, this molecule is discussed in the other chapters of this report.

3.1.1. Au (111) Surface Reconstruction

Reconstruction of the (111) surface of Au is typically performed by sputtering of the surface with Argon followed by annealing at 625°C.[2] When properly prepared, the classic herringbone feature is visible.[3] The herringbone reconstruction on Au (111) provides a suitable template for preparation of organic monolayer whose surface chemistry can also be studied with STM. In the present study a monolayer of metal phthalocyanine (MPc) was deposited by organic molecular beam epitaxy (OMBE) on the Au (111) surface. A properly prepared Au (111) has a readily observed herringbone reconstruction surface both on the bare surface and on the MPc covered surface as shown in Fig 1, images obtained by Dr. Sangyeob Lee, James Royer and Jun Park using author designed annealing system.

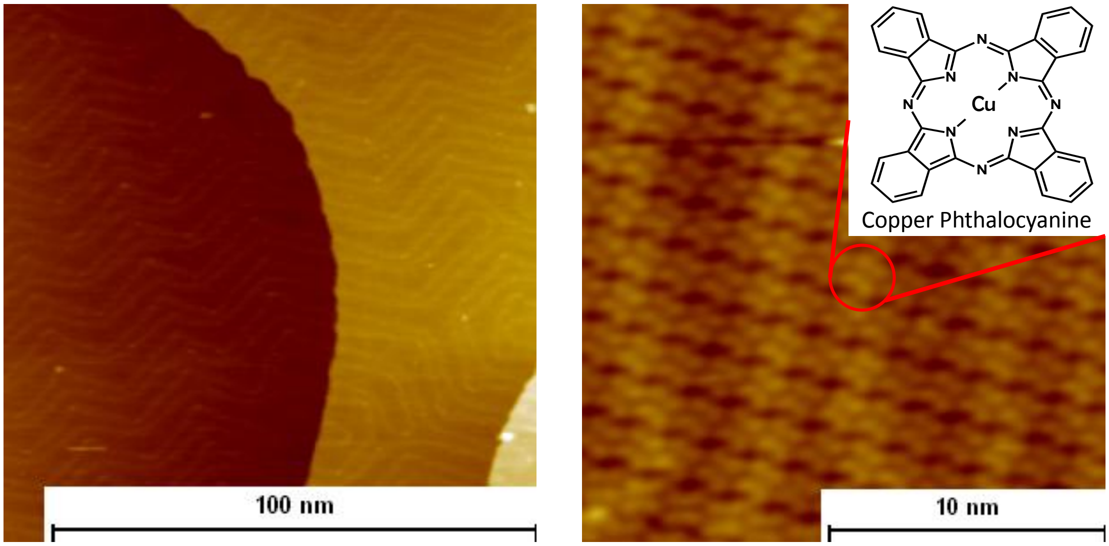

Figure 3.1: STM of Au surface, note the herringbone structure (Left), STM of a monolayer of Copper Phthalocyanine on Au, herringbone structure still visible (Right)

3.1.2. Si (001) Surface Reconstruction

Surface preparation of Si (001) samples involves several steps; the oxide layer and carbon contaminants must be removed, from the surface to allow the surface to form an ordered low defect density reconstruction. While there are different ways of preparing a Si surface, this study focused on the technique of Swartzentruber *et al:* "flashing" the Si sample followed by annealing.[4] This thermal profile steps through a series of temperatures in order to remove the SiO_2 layer, diffuse carbon into the bulk material, and anneal the surface. The specific temperatures were based on the work of Owen as illustrated in Figure 3.2.[5]

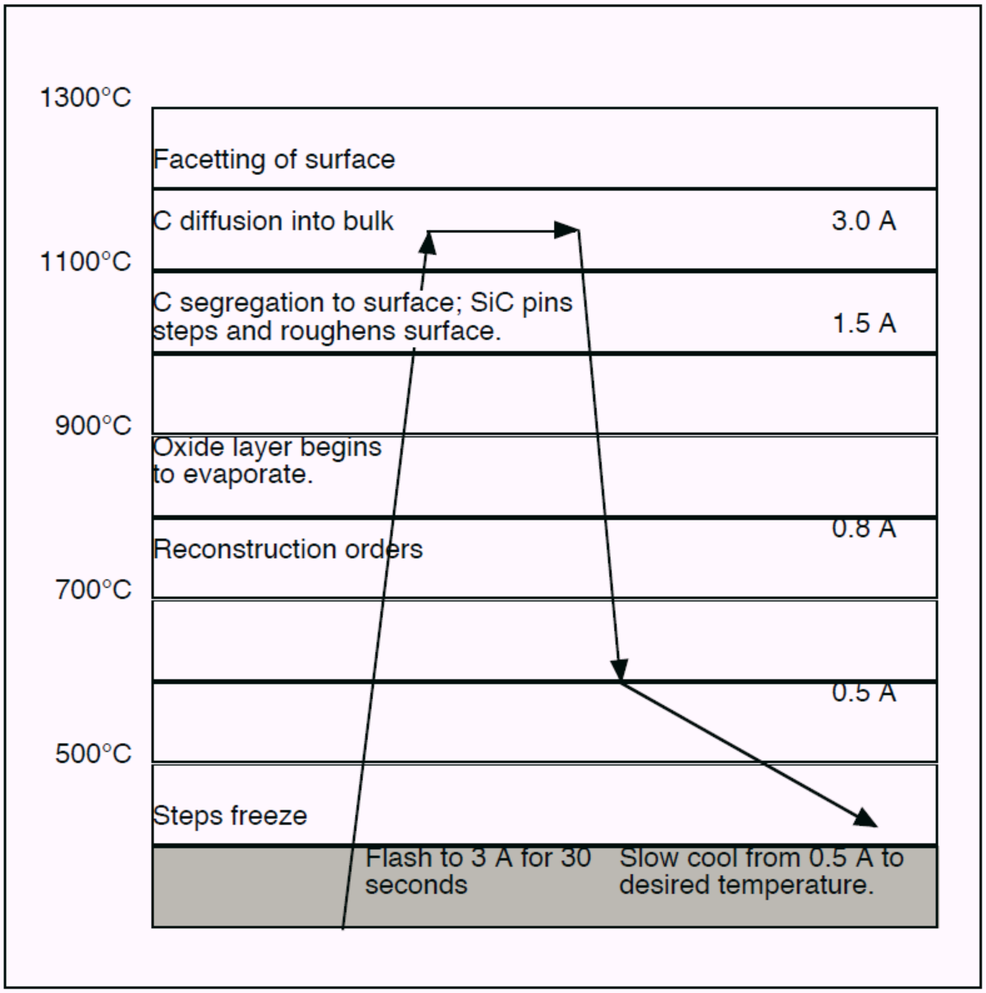

Figure 3.2: Typical heat treatment profile for Si surface reconstruction. [5]

The SiO_2 oxide layer present in Si begins to evaporate as Si is raised above temperatures of 825°C .[6] At temperatures above 925°C, carbon segregates to the surface in the form of SiC while at temperatures above 1125°C the SiC dissolves back into the bulk silicon.[6] Too much heat can be detrimental and at temperature above 1225°C the Si surface begins to facet. A Si surface properly flashed and annealed is shown in Figure 3.3, image obtained by Dr. Sangyeob Lee, James Royer and Jun Park using author designed annealing system. The image shows ordered Si rows, consistent with the desired 2x1 reconstruction for Si (001) samples. A clean Si (001) 2x1 reconstruction provides an ideal test surface for STM tip preparation due to the simple surface structure and ability to achieve atomically resolved images.

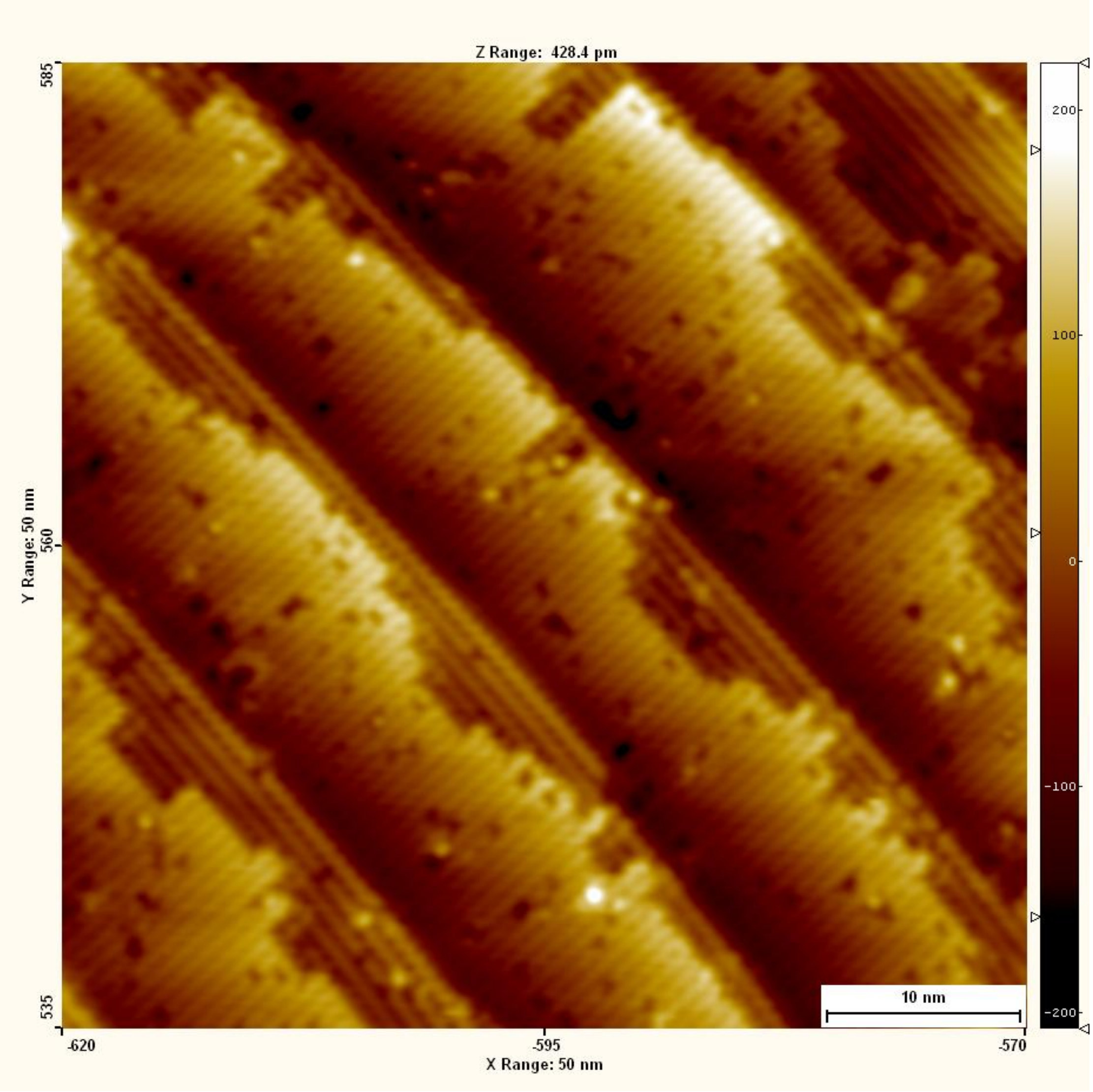

Figure 3.3: High Resolution STM of Si with step edges

3.1.3. PID Control Loop History and Theory

Since the value of heating to specific temperature profiles has been established, the controllers used to generate heating profiles will be examined. Proportional-Integral-Derivative (PID) controllers are one type of feedback control loop. The PID feedback controller has a long history and applications go back as far as Minorsky's work on the automatic steering of the naval ship USS *New Mexico* in 1922.[7] An analog PID controller was able to steer the *USS New Mexico* to within ±0.6° of its desired heading, better than most helmsmen could achieve.[8] Regardless of its performance, the Navy did not embrace automatic steering and Minorsky's PID controller was removed from the USS *New Mexico* upon completion of testing. [9]

A PID controller compares the present error between a measured process variable and a desired set point, but it also compares error history as well as a prediction of future errors to generate a gain that is applied to a manipulated variable. The PID performs these actions by integrating and differentiating the error to yield three portions of the PID control equation, see Figure 3.4.

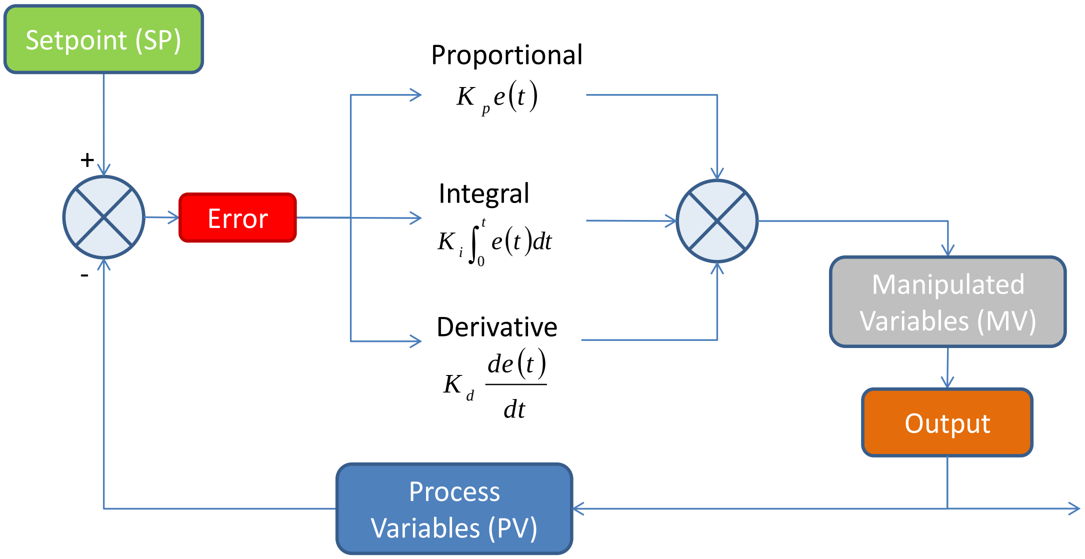

Figure 3.4: PID controller block diagram. Set point is compared with output, resulting error scaled, integrated and has the derivative taken. Summed gains are applied to the process variable which changes the output of the system.

There are several variables in PID control, the first is the process variable (PV), which is the variable that is being measured, in this study the PV is sample temperature. The second variable is the set point (SP) which is the desired temperature profile in this study. The last variable is the manipulated variable (MV) to which changes are made to control the system, which is the output current from the power supply is the MV in this study. Gain values of K_P, K_i, and K_d are applied to their respective portions of the PID loop. These are also the parameters by which a PID loop is "tuned" to specific system.

3.2. Hardware

Figure 3.5 depicts a general setup for the temperature controller. The main components of the system are the UHV chamber, the electronics equipment rack and a PC computer running the control software.

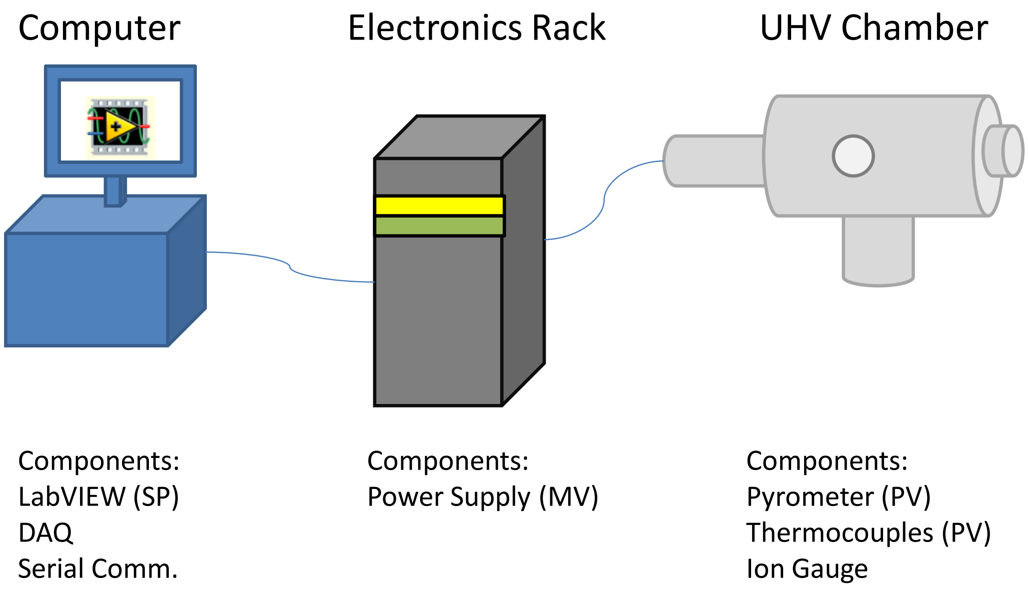

Figure 3.5: Major components of the temperature controller used in PID feedback loop. The computer generates a set point (SP), the power supply regulates the Manipulated Variable (MV) of current, the Pyrometer or thermocouples measure the Process Variable (PV) of temperature

3.3. UHV Chamber

The UHV chamber is a custom built Omicron chamber capable of performing several types of analysis in addition to STM. Two main chambers are the preparation chamber and the scanning chamber. All annealing is carried out in the preparation chamber. UHV chamber pressure is measured with a hot cathode ionization gauge and is maintained at 2 x 10^{-10} Torr. Instruments related to annealing Inside the UHV chamber include the thermocouples, pressure gauges and a Pyrolytic Boron Nitride (PBN) heater. Temperature measurements are taken either by an Ircon Modline 5 Model 5G-1415 infrared thermometer sensor or by thermocouples. This infrared thermometer is mounted on the exterior of the chamber but can measure the surface temperature of a sample inside the chamber from a distance of 24 cm. Two standard K-type thermocouples are mounted on the transfer arm that holds the sample, since these thermocouples are not in direct contract with the sample; therefore, they are not the preferred method of temperature measurement. A thermocouple is a junction between two different types of metal that produces a voltage proportional to a temperature difference. Direct thermocouple contact to the sample is not possible since the sample must be free of wires in order to have vibration-free STM imaging.

3.3.1. Electronics Rack

The electronics rack houses the power supply, thermocouple and pyrometer control units as well as the control unit for the hot cathode ionization gauge. A TDK Lambda Gen 60-12.5 power supply supplies the necessary current to heat the sample. This power supply has voltage range of 0-60V and a current range of 0-12.5A. A custom built housing assembly holds the thermocouple display unit as well as the pyrometer display unit.

3.3.2. PC

All operations are controlled by a PC using LabVIEW. The PC communicates with the electronics rack through both digital and analog communication. Chamber pressure, thermocouples and the IR thermometer are measured from the rack by the computer through an analog signal of 0-10V. Connections are made through a National Instruments BNC-2110 connection block connected to a NI PCI-6251 DAQ. RS-485 Communication with the power supply is achieved with a PCI-8433/4 High-Performance, Isolated 4-Port PCI Serial Interface.

3.4. PID Feedback Control via LabVIEW Software

3.4.1. LabVIEW PID Overview and Operation

The PC running LabVIEW controls the annealing system. Simply, the PC compares temperature measurements of the sample to a desired set point and adjusts current from the power output to minimize the difference. Error in temperature is controlled by heating or cooling the sample. Two methods exist for heating the sample, direct and indirect. In the direct method, current flows directly through the sample to generate heat, this method is more appropriate for a Si sample. Direct heating requires samples to have a finite resistance so it works well for most semiconductor samples but does not work for insulator and metal samples. Samples not appropriate for direct heating are heated indirectly by a nearby heater. Current flows through a resistive element known as PBN heater to heat the sample which is in close proximity. Indirect heating is more appropriate for Au samples.

The custom built LabVIEW program employs standard PID measures to control sample temperature. The LabVIEW program has two main portions, one portion measures user inputs, temperature, pressure and power supply data while the second portion generates set points and performs PID feedback. The program continuously gathers state data inside one loop, then passes those variables to the PID control loop which evaluates each point, and provides corrections to the manipulated variable. The block diagram of the two loops is seen in Figure 3.6.

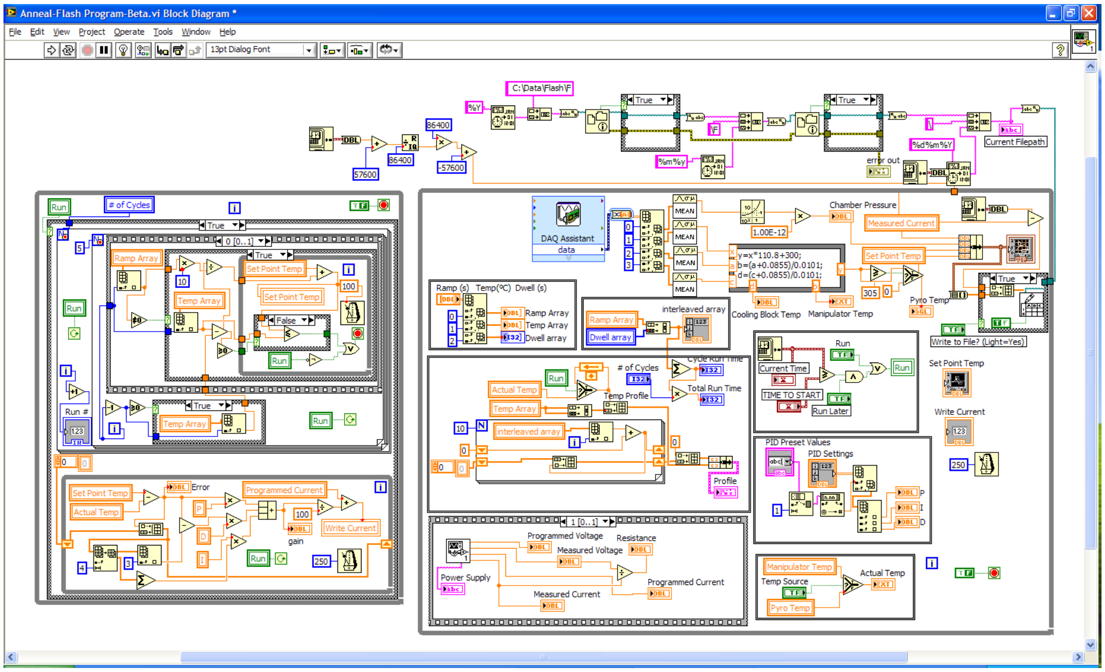

Figure 3.6: Block Diagram of PID controller, PID loop and set point generator in left side loop, process variable and manipulation variable on Right hand side loop.

Users can customize the annealing system such as selecting the pyrometer or thermocouple as the process variable temperature source. Pyrometer temperature readings are instantaneous and are appropriate for very responsive samples like silicon. Thermocouple temperature measurements are made several millimeters away from the sample on a different surface and require several minutes to stabilize to the actual surface temperature. The LabVIEW program even offers a non-feedback control option where current is controlled directly by the user entered profile regardless of the measured temperature, this is known as open-loop control method.

3.4.2. Temperature Set Point Profile Determination

Any anneal/flash profile can be requested of the program. A profile typically consists of a ramp to a temperature set point, a hold at that temperature, and a ramp to the next temperature set point. Users can set up to five set points during the profile to allow for various holds at desired temperatures. After a user sets a determined anneal/flash profile, the program runs in feedback mode minimizing the error between the sample temperature and the set point temperate defined by the profile. Users can set the program to repeat the temperature profile any number of times. See Figure 3.7 for a typical annealing profile for Si surface reconstruction.

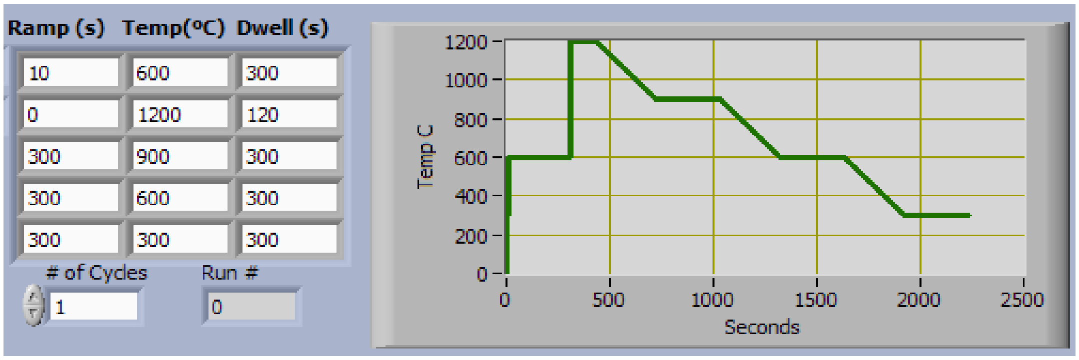

Ramp (s)	Temp(ºC)	Dwell (s)
10	600	300
0	1200	120
300	900	300
300	600	300
300	300	300

# of Cycles: 1

Run #: 0

Figure 3.7: Typical annealing profile for Si reconstruction, user set desired set points (Left), LabVIEW generates a temp profile (Right)

3.4.3. Process and Manipulation Variable

A data acquisition device (DAQ) is required to measure the values of pressure and temperature. These values are expressed as an analog voltage between 0-10V which is measured by a National Instruments PCI-6251 DAQ. The DAQ takes 1000 samples at 5 kHz every 250 milliseconds for each pressure and temperature channel. LabVIEW programming applies an equation to turn that voltage value into an engineering unit.

In addition of temperature and pressure data, the PC communicates via RS-485 communication protocol with the power supply. Every 250 milliseconds the PC receives the power supply's current output and replies with a new current output. While in feedback mode, the PC all sends commands to the power supply to set desired current output level. Current output is the only output from the PID control loop.

3.4.4. LabVIEW PID Control Loop

A custom made LabVIEW PID loop was made for the system; the proportional (P) portion of the loop compares the actual temperature of the sample to the desired temperature as set by the temperature profile. The difference between these values is multiplied by the proportional gain and applied to the MV. The Integral (I) portion of the loop integrates the error over time by summing the last 5 error values, this value is multiplied by the integral gain and applied to the MV. The derivative portion of the loop calculates the rate of change of error with, this value is multiplied by the derivative gain and applied to the MV. Block diagram of PID shown in Figure 3.8.

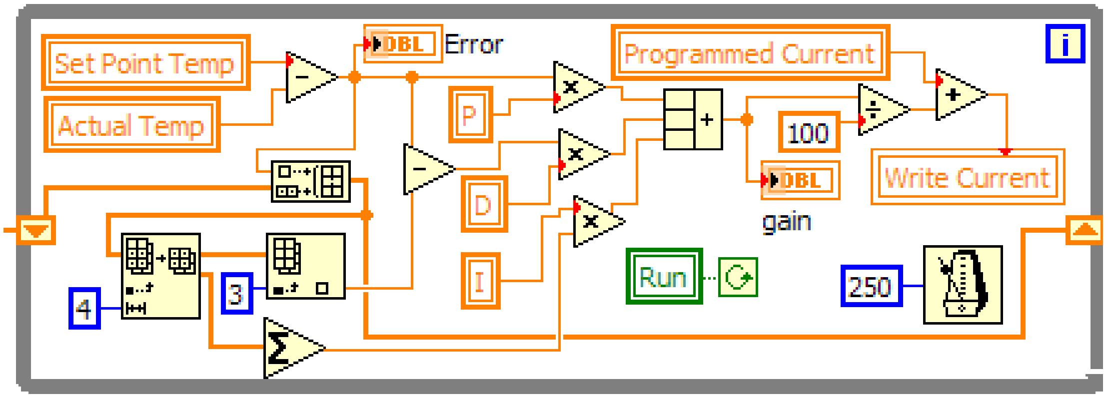

Figure 3.8: PID loop Block Diagram

Every PID loop uses gain variables. The Ziegler-Nichols methods is a popular method for tuning PID parameters and was developed in the 1940s.[10] The Ziegler-Nichols method raises the proportional gain until the system becomes unstable then uses the period and proportional gain values to set the integral and derivative gains. Tuning of the system in this study followed the Ziegler-Nichols method approximately. Step inputs of 100°C and 200°C were performed to determine optimal gain parameters of the system. PID parameters for this system were not optimal at all temperatures. At higher temperatures the system was naturally more damped. When high temperature PID gains were used the system became under damped at low temperatures causing overshoots of the set point.

3.5. Conclusion

A custom built PID annealing system was designed to automate control for heating profiles of Si and Au samples. This setup performed surface reconstruction on Si (001) and Au (111) samples. These samples were then imaged by STM to reveal high order surfaces. The automated program dramatically reduces the required man-hours invested in UHV sample preparation and provides significantly more accurate temperature control than manually controlled flashing/annealing methods.

3.6. References

1. Binnig, G., et al., *Surface Studies by Scanning Tunneling Microscopy.* Physical Review Letters, 1982. **49**(1): p. 57.

2. Barth, J.V., et al., *Scanning tunneling microscopy observations on the reconstructed Au(111) surface: Atomic structure, long-range superstructure, rotational domains, and surface defects.* Physical Review B, 1990. **42**(15): p. 9307.

3. Cheng, Z.H., et al., *Adsorption Behavior of Iron Phthalocyanine on Au(111) Surface at Submonolayer Coverage.* The Journal of Physical Chemistry C, 2007. **111**(26): p. 9240-9244.

4. Swartzentruber, B.S., et al., *Scanning tunneling microscopy studies of structural disorder and steps on Si surfaces.* Journal of Vacuum Science & Technology A: Vacuum, Surfaces, and Films, 1989. **7**(4): p. 2901-2905.

5. Owen, J.H.G., *The Adsorption, Diffusion and Reaction of Small Adsorbates on the Si(001) surface*, in *Department of Materials*. 1996, Oxford University. p. 151.

6. Dijkkamp, D., et al., *Scanning tunneling microscopy study of Si (001) and Si (110) surface structures resulting from different thermal cleaning treatments.* Journal of Vacuum Science & Technology A: Vacuum, Surfaces, and Films, 1990. **8**(1): p. 218-221.

7. Minorsky, N., *DIRECTIONAL STABILITY OF AUTOMATICALLY STEERED BODIES.* Journal of the American Society for Naval Engineers, 1922. **34**(2): p. 280-309.

8. Bennett, S., *A history of control engineering 1800-1930*. 1979, London: Peter Peregrinus. 219.

9. Bennett, S., *Nicholas Minorsky and the automatic steering of ships.* Control Systems Magazine, IEEE, 1984. **4**(4): p. 10-15.

10. Ziegler, J.G.a.N., N. B., *Optimum settings for automatic controllers.* Transactions of the ASME, 1942. **64**: p. 759–768.